ACS APPLIED ENERGY MATERIALS
Cite This: ACS Appl. Energy Mater. 2019, 2, 8535−8549
Article
www.acsaem.org

Leveraging Nanoparticle Dispersion State To Tune Vanadium Ion Selectivity of Nanophase-Segregated Ionomer Nanocomposites for Redox Flow Batteries

Allison Domhoff,[†] Apoorv Balwani,[†] Tyler B. Martin,[‡] and Eric M. Davis*[,†]

[†]Department of Chemical and Biomolecular Engineering, Clemson University, Clemson, South Carolina 29634, United States
[‡]National Institute of Standards and Technology (NIST) Center for Neutron Research (NCNR), Gaithersburg, Maryland 20899, United States

Supporting Information

ABSTRACT: Ionomer nanocomposites provide a promising solution to address ion crossover issues inherent to traditional ion-containing membranes used in batteries for grid-scale energy storage (e.g., vanadium redox flow batteries). Herein, we investigate the impact of nanoparticle surface chemistry on nanoparticle dispersion, membrane morphology, and vanadium ion permeability in a series of Nafion nanocomposites. Specifically, silica nanoparticles (SiNPs) were functionalized with various chemical moieties, seven in total, that electrostatically interact, either attractively or repulsively, with the sulfonic acid groups that coalesce to form the ionic network within Nafion. As seen from electron microscopy analysis of the nanocomposites, SiNPs with sulfonic acid end-functionality were, on average, well dispersed within the ionomer membrane, though increased vanadium ion permeability, as compared to pristine (or unmodified) Nafion, was observed and attributed to changes in the Donnan potential of the system. In contrast, SiNPs with amine end-functionality were, on average, observed to form large aggregates within the ionomer membrane. Surprisingly, nanocomposites containing a higher degree of nanoparticle aggregation demonstrated the lowest vanadium ion permeability. Fractal analysis of the low-Q small-angle neutron scattering data suggests that the interface between the ionomer and the SiNP surface transitions from rough to smooth when the nanoparticle surface is changed from sulfonic acid-functionalized to amine-functionalized.

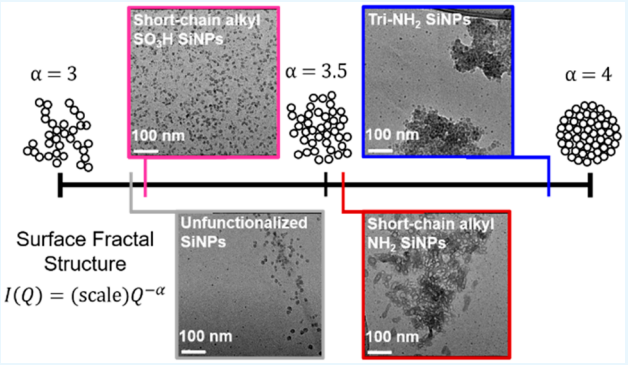

KEYWORDS: *ionomer nanocomposites, morphology, redox flow batteries, ion crossover, SANS*

INTRODUCTION

Nafion, the current state-of-the-art polymer electrolyte membrane for vanadium redox flow batteries (VRFBs),[1,2] is a nanophase-segregated ionomer containing a hydrophobic Teflon-like backbone with hydrophilic sulfonic acid-terminated pendant chains.[3−5] The backbone provides chemical, mechanical, and thermal stability, while the ionic groups, in the presence of water, coalesce to form an interconnected ionic network that allows for facile cation transport through the membrane.[1,6,7] However, one standing issue with Nafion is its poor ion selectivity.[4,8] That is, Nafion suffers from high vanadium ion crossover between vanadium electrolyte solutions, reducing the overall potential and ultimately the lifetime of the battery.[9] In efforts to increase the ion selectivity for protons in Nafion, several modification routes have been pursued.[8,10−13]

Most notably, the incorporation of nanoparticles (NPs), typically silica nanoparticles (SiNPs), into the Nafion membrane has been widely explored.[3,8,13−15] The Nafion−SiNP composite membranes investigated, to date, have primarily utilized a procedure known as sol−gel condensation,[3,8] whereby a solid Nafion membrane is immersed in a solution containing NP precursors, which diffuse into the membrane and react to form an inorganic silica phase within the extruded film.[14,16] While this modification method allows for greater scalability, control over the sol−gel condensation process is limited, resulting in a silica phase that is not well dispersed within the membrane and is quite heterogeneous (in both size and shape).[3,17] Alternatively, nanocomposite membranes can be fabricated by using a solution-cast method. For this method, solid SiNPs of specific size and surface chemistry are added to a polymer dispersion, after which the dispersion is cast, and the solvent is allowed to evaporate, forming a dense, nanocomposite membrane.[15,18,19] This fabrication method allows for greater control over both the size and surface functionality of the silica phase in the resulting

Received: July 24, 2019
Accepted: November 11, 2019
Published: November 11, 2019

DOI: 10.1021/acsaem.9b01443
ACS Appl. Energy Mater. 2019, 2, 8535−8549

ionomer composite. Both of these fabrication routes have created composite membranes that exhibit reduced vanadium ion crossover (approximately a 3−4-fold reduction) as compared to Nafion with no silica.[8,13,20]

It has been hypothesized that the NPs reside within the ionic domain of Nafion and act to sterically block the passage of hydrated vanadium ions, while still allowing facile transport of smaller protons (or hydronium ions) through the membrane.[8,13,21,22] However, recent small-angle neutron scattering (SANS), small-angle X-ray scattering (SAXS), and transmission electron microscopy (TEM) investigations on sol−gel fabricated ionomer nanocomposites have found that the NPs are, on average, much larger (100s of nm in diameter) than the ionic domains in Nafion, which are on the order of 3−5 nm in size, casting doubt on the proposed mechanism of sterically hindered vanadium ion transport.[3,17,23] Additionally, recent work from our group showed that the surface chemistry of the SiNP governed the dispersion of the NPs within the ionomer, which in turn affected the permeability of vanadium ions across the membrane, where nanocomposite membranes with the highest NP aggregation showed the greatest reduction in vanadium ion permeability.[20] While this recent study underscores the importance of nanoparticle dispersion and surface chemistry on the observed performance of these ionomer nanocomposites, only a limited number nanoparticle surface functionalizations were explored.

In other nanophase-segregated polymers, such as block polymers, the dispersion of NPs within the film has been investigated as a means to modify mechanical properties of the pristine block polymer.[24] The so-called "dispersion state"[25] of the NPs can be manipulated by adjusting the NP type, surface functionality, size, and shape, allowing the NPs to, for example, segregate into one phase of a nanophase-segregated system or even act as a surfactant between polymer phases.[26] Generally, modifications to the NP type and surface functionalization are used to prevent NP aggregation (or clustering) by promoting favorable interactions between the NP and polymer matrix, thus creating more uniform dispersions.[24] Favorable interactions, or lack thereof, can often be predicted by the fundamental theory proposed by Deryagin, Landau, Verwey, and Overbeck (or DLVO theory), which describes NP interactions in solution. DLVO theory may also help predict the dispersion of NPs in solution cast membranes, as it suggests that through the interplay between van der Waals attractive forces, electrostatic repulsive stabilization, and steric separation, the NP dispersion within the solution can be directly controlled.[27]

An electrosterically stabilized (i.e., a combination of charge and steric effects) particle is protected by an external layer that minimizes particle aggregation, either by the way of an electrostatic layer or a physically adsorbed layer.[28,29] The high surface energy of unmodified NPs facilitates agglomeration if the stabilizing attributes predicted by DLVO theory are not met. Chemical modification of particles has been shown to minimize particle−particle interactions, as well as enhance particle−matrix interactions, allowing the polymer to better "wet" the NP surface.[30−32] Furthermore, the size and shape of the NP affect the conformational entropy of the polymer, as the polymer chains are forced to twist and stretch around the rigid filler. As a result, large NPs without favorable interactions may be expelled from the polymer bulk matrix entirely.[24] However, as the final NP dispersion state within the membrane is governed by both entropic and enthalpic contributions, simply promoting strong interactions between the NPs and the polymer matrix does not necessarily lead to nanocomposites with well-dispersed NPs. Recent molecular dynamics simulations performed by Cheng and Grest[33] demonstrated that strong particle−matrix interactions may lead to NPs accumulating at the solvent evaporation interface, whereas NPs that are only partially wetted by the polymer matrix are more uniformly distributed in the bulk polymer. Additionally, it is well-known that numerous other processing factors affect the dispersion of NPs in a composite film fabricated by solution casting, including rate of solvent evaporation, type of solvent, and mixing mechanism.[34−37]

Herein, we investigate the impact of nanoparticle surface chemistry on the dispersion of SiNPs in Nafion and, further, its impact on the vanadium ion permeability of these ionomer nanocomposites. Specifically, SiNPs were functionalized with seven different chemical moieties, which represent different electrosteric-stabilizing effects described by DLVO theory. The surface of the NPs was modified with end groups that interact electrostatically, either repulsively or attractively, with the sulfonic acid (ionic) groups of Nafion. Additionally, the flexibility and length of the bridging chain between nanoparticle surface and terminating end group were varied. Successful functionalization of the SiNP surface was confirmed by both Fourier transform infrared (FTIR) spectroscopy and zeta-potential measurements, after which the functionalized NPs were incorporated into Nafion membranes via solution casting. The morphology of the nanocomposite membranes was obtained by both TEM imaging and SANS measurements on hydrated membranes. Contrast-matched SANS measurements were performed to gain additional insight into the fractal nature of the silica−polymer interface within the ionomer nanocomposite. Furthermore, the vanadium ion permeability was measured by ultraviolet−visible (UV−vis) spectroscopy and related to the SiNP dispersion state of the ionomer nanocomposite membranes.

EXPERIMENTAL SECTION

Materials. Ethanol (pure, 200 proof, anhydrous), sulfuric acid (95%−98% ACS Reagent), fuming sulfuric acid (reagent grade), (3-mercaptopropyl)trimethoxysilane (95%) (MPTMS), Nafion stock solution (Nafion DE 2021, w_{Nafion} = 20% in mixture of lower aliphatic alcohols and water), and tin(II) chloride (reagent grade, 98%) ($SnCl_2$) were purchased from Sigma-Aldrich. Methyl isobutyl ketone (certified ACS solvent) (MIBK) was purchased from Fisher Scientific. Glycidyl phenyl ether (99%) (GPE) was purchased from Acros Organics. Hydrogen peroxide (30%) was purchased from VWR Analytical. 3-Aminopropyltrimethoxysilane (97+ %) (APTMS) was purchased from TCI Chemicals. *p*-Aminophenyltrimethoxysilane (*p*-APhTMS) was purchased from Manchester Organics. (3-Trimethoxysilylpropyl)diethylenetriamine (TMSDEA), 11-aminoundecyltriethoxysilane (AUTES), and 11-mercaptoundecyltrimethoxysilane (MUTMS) were purchased from Gelest. Unfunctionalized SiNPs (colloidal silica in methanol; MTST grade; $D_{P,avg}$ = 11 nm) were obtained from Nissan Nanomaterials. Note, the variable "*w*" will be used from this point forward to represent mass percent, i.e., (mass of *X*/total mass) × 100%.

Short-Chain Alkyl−SO_3 (AS-SiNP) and Long-Chain Alkyl−SO_3 (LS-SiNP) Nanoparticle Functionalization. To a solution of deionized water (50 mL) and ethanol (50 mL), silica NPs (500 mg of solids, as MT-ST at w_{NP} = 30.6%) were added. The mixture was sonicated for 1 h, silane (2 mL of MPTMS for AS-SiNP or 0.5 mL of MUTMS for LS-SiNP) was added dropwise, and the solution was refluxed overnight. The alkylthiol−SiNPs were centrifuged (1361 rad s^{-1}, 20 min) and washed three times with water. The wet NPs were then stirred in a solution of water (40 mL), methanol (40 mL), and

DOI: 10.1021/acsaem.9b01443
ACS Appl. Energy Mater. 2019, 2, 8535−8549

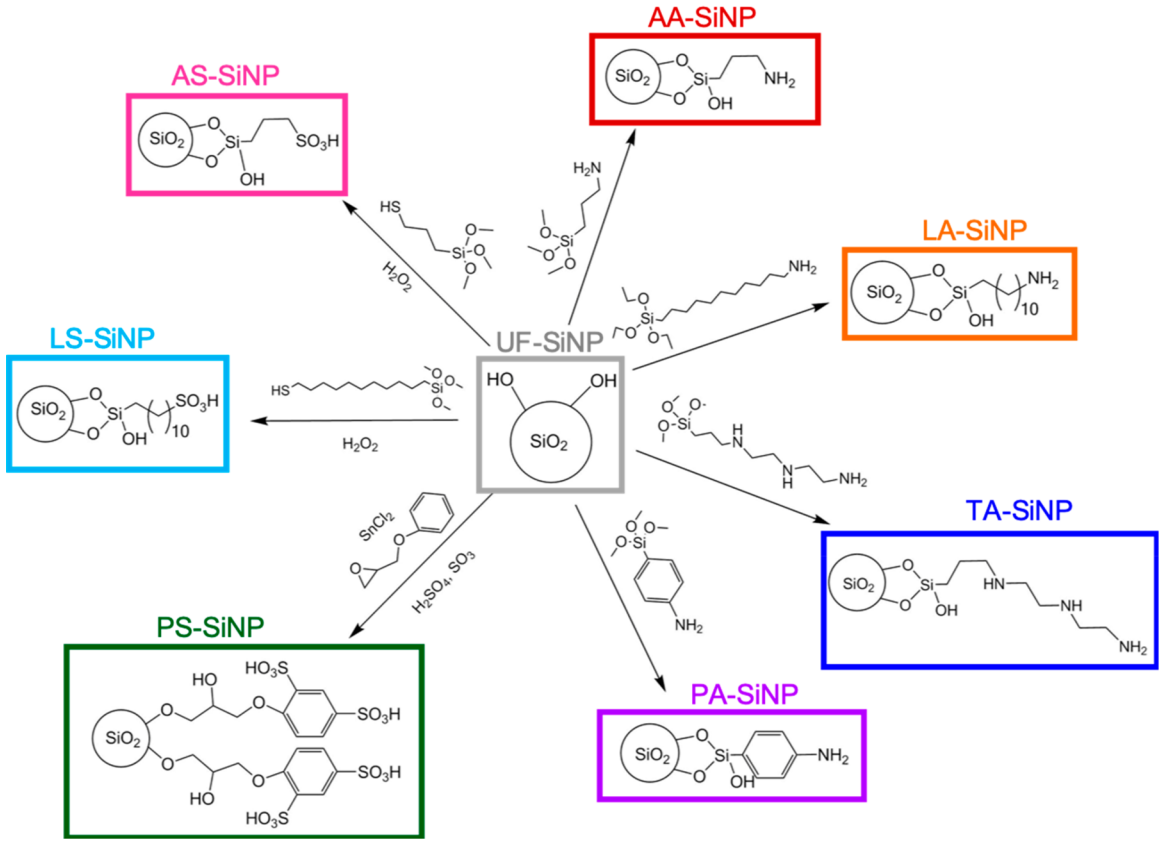

Figure 1. Reaction scheme for various SiNP surface functionalizations.

30% H_2O_2 (40 mL) at room temperature for 24 h. The NPs were again centrifuged and washed with water. After evaporating the water in the hood overnight, the dry NPs were stirred in a solution of 1 mol L^{-1} H_2SO_4 for 3 h and further centrifuged and washed. The NPs were left in solution to avoid further aggregation.

Phenyl-SO_3 (PS-SiNP) Nanoparticle Functionalization. By use of a method previously developed,[38] SiNPs (500 mg of solids, as MT-ST at w_{NP} = 30.6%) were dried and redispersed as a w_{NP} = 15% solution in MIBK via sonication. GPE (1.25 g) was added to the NP suspension, and the solution was briefly sonicated. Following this, 0.100 mol % (relative to GPE) $SnCl_2$ catalyst was added, and the solution was magnetically stirred for 3 h at 140 °C. Subsequently, the NP solution was cooled, centrifuged (1361 rad s^{-1}, 20 min), and then washed with DI water twice. The wet NPs were treated with fuming sulfuric acid (1.63 g) at room temperature, and the solution was stirred for 18 h. The reaction was ceased by pouring the NP solution into an ice water bath. The precipitate was collected by centrifugation (1518 rad s^{-1}, 30 min) and washed with water. The NPs were left in solution to avoid further aggregation.

Short-Chain Alkylamine (AA-SiNP), Phenylamine (PA-SiNP), Triamine (TA-SiNP), and Long-Chain Alkylamine (LA-SiNP) Nanoparticle Functionalization. To a round-bottom flask, ethanol (150 mL), water (10 mL), and SiNPs (500 mg of solids, as MTST at w_{NP} = 30.6%) were added, and the flask was capped with rubber septum. The solution was then sonicated for 30 min. After sonication to suspend and dilute NP solution, silane (35 μL of APTMS for AA-SiNP, TMSDEA for TA-SiNP, AUTES for LA-SiNP, or 0.05 g of *p*-APhTMS for PA-SiNP) was added through the septum to the solution. The reactions of AA-SiNP, PA-SiNP, and TA-SiNP were stirred for 24 h at room temperature, and LA-SiNP reaction was stirred for 5 days. After the reaction time, the solution was centrifuged (1361 rad s^{-1}, 20 min) and washed three times with water. The NPs were left in solution to avoid further aggregation.

Nanocomposite Membrane Solution Casting. All nanocomposite membranes were cast from the as-received Nafion stock solution. To incorporate the NPs, various amounts of SiNPs (both unmodified and each of the surface functionalized) were suspended in Nafion solution by sonication for at least 30 min prior to casting. The SiNP−Nafion suspensions were then cast onto quartz windows, covered by a funnel with Kim-wipe flue, and allowed to evaporate overnight. The dried hybrid films were then annealed at 140 °C for 2 h under dynamic vacuum, then the heat was shutoff, and after 30 min the films were left under static vacuum to cool to room temperature. The films were hydrated in DI water overnight before further use. The hydrated film thickness was on the order of (20−50) μm.

Vanadium Crossover Experiments. Vanadium ion crossover was measured as previously described.[20] Briefly, a tailor-made diffusion cell (Permegear Franz cell, Bethlehem, PA) was used; the receiving cell, volume 15 mL, was filled with 1.5 mol L^{-1} $MgSO_4$ in 3 mol L^{-1} H_2SO_4, and the donating cell, volume 1 mL, was filled with 1.5 mol L^{-1} $VOSO_4$ in 3 mol L^{-1} H_2SO_4 with membrane sandwiched between the cells. Aliquots were sampled via the side arm of the receiving cell at regular time intervals. The concentration of vanadium(IV) ions was measured with a UV−vis spectrometer (VWR UV-3100PC) from (400−1100) nm. The peak associated with V^{4+} can clearly be observed at 760 nm. Following UV−vis characterization, the aliquots were placed back into the receiving cell. From these data, the permeability of vanadium ions can be calculated from the equation

$$V_R \frac{dC_R(t)}{dt} = A\frac{P}{L}C_D \quad (1)$$

where C_D and $C_R(t)$ are the vanadium ion concentration in the donating and receiving cells, respectively, A and L are the area and thickness of the membrane, respectively, P is the permeability of vanadium ions (cm^2 s^{-1}), and V_R is the volume of the receiving cell. This expression assumes that (1) the permeation in the membrane has reached a pseudo-steady state, (2) vanadium ion permeability is independent of ion concentration, (3) $C_D \gg C_R(t)$, and (4) the reduction in C_D over the length of the experiment is negligible.[39]

DOI: 10.1021/acsaem.9b01443
ACS Appl. Energy Mater. 2019, 2, 8535−8549

Nanoparticle Analysis. Nanoparticle functionalization was analyzed by Fourier transform infrared spectroscopy (FTIR) using a Thermo Scientific Nicolet iS50R FT-IR equipped with Golden Gate attenuated total reflectance (ATR) attachment (diamond ATR crystal, 64 scans, resolution of 4 cm^{-1}, background taken before each sample). Nanoparticle surface chemistry was further analyzed by measuring the zeta-potential under acidic pH (in this case, pH ≈ 2) with a Malvern Zetasizer Nanoseries (Nano-ZS). This pH was selected based on the apparent pH of Nafion stock solution (pH ≈ 2), which was measured by a Hach Sension 5048 pH probe. To prevent sedimentation of less stable dispersions, zeta-potential measurements were taken immediately following sonification of each solution.

High-Resolution Transmission Electron Microscopy. Transmission electron microscopy (TEM) nanocomposite film samples were made by drop-casting solutions of w_{Nafion} = 0.05%−0.1% composite Nafion in ethanol onto lacey carbon girds (Electron Microscopy Services, Hatfield, PA) and allowed to dry for at least 24 h. Samples were analyzed on Hitachi 9500 high-resolution TEM (HR-TEM) operated at 300 kV, emission current of 8.0 μA, and filament at 29.1 V with an exposure time of 2.0 s. ImageJ was utilized to determine particle size.[40]

Small-Angle Neutron Scattering (SANS). SANS experiments were performed on the NG-B 10 m SANS (Figures 3−5, pristine Nafion data in Figure 6) and the NG-7 30 m SANS (all SANS curves in Figure 6 except pristine Nafion) at the National Institute of Standards and Technology Center for Neutron Research (NCNR).[41] Nanocomposite films were cast and annealed as previously described and hydrated by H_2O or H_2O:D_2O solution (24:76 by volume) for 24 h before analysis. The hydrated films were then placed in a demountable cell, where the distance between quartz windows was 1 mm. A circular aperture with diameter of 0.5 cm was utilized for all samples except the LS-SiNP sample hydrated in pure water, which utilized a circular aperture of 0.25 cm due to smaller sample size. The incoming neutron wavelength and the sample-to-detector distance were varied to collect a range of $Q = 4\pi \sin(\theta)/\lambda$ values, with θ representing the scattering angle and λ the neutron wavelength. Q values were collected ranging from (0.0035−0.5) $Å^{-1}$ for the 10 m SANS and (0.0009−0.5) $Å^{-1}$ for the 30 m SANS. The total collection time for each sample was ∼3 h. The SANS data were reduced by using the software package developed at the NIST Center for Neutron Research,[42] where the thickness of the cell was used for the reduction calculations.

RESULTS AND DISCUSSION

Nanoparticle Functionalization. The reaction scheme for each of the nanoparticle functionalizations is shown in Figure 1. Also, the nomenclature assigned to each surface functionalization has been summarized in Table 1. Note, the color scheme and nomenclature for each of the SiNP surface chemistries shown in Figure 1 and Table 1 will be used for the remainder of the article. As seen from the schematic in Figure 1, the surface modifications to the unfunctionalized (i.e., hydroxyl-coated) SiNPs (shown in the center gray box) have been chosen to contain either sulfonic acid (i.e., SO_3H) or amine (i.e., NH_2) end-functionality. The negatively charged sulfonic acid end-functionality is chemically identical to the sulfonic acid groups terminating the pendant chains of Nafion and is therefore expected to repulsively interact with the ionic phase of Nafion. In contrast, the positively charged (under the acidic conditions within Nafion) amine functionality is expected to attractively interact with the sulfonic groups in the ionic phase of Nafion. In addition, within each end-functionality, the bridging chain between the SiNP surface and the terminating group was adjusted. Specifically, a rigid phenyl-containing chain (PA-SiNP and PS-SiNP), a semiflexible short alkyl chain (3 carbons; AA-SiNP and AS-SiNP), and a flexible long alkyl chain (11 carbons; LA-SiNP and LS-SiNP) were selected. In addition, a fourth amine functionalization was chosen, which contained both a terminal amine group and two amine groups along the alkyl chain (TA-SiNP). These surface modifications allow us to systematically investigate both charge and steric stabilization on the final SiNP dispersion state within the ionomer nanocomposite.

Table 1. Nomenclature for Unfunctionalized and Functionalized SiO_2 Nanoparticles

SiNP surface chemistry	nomenclature
unfunctionalized	UF-SiNP
short-chain alkylamine	AA-SiNP
phenylamine	PA-SiNP
triamine	TA-SiNP
long-chain alkylamine	LA-SiNP
short-chain alkylsulfonic acid	AS-SiNP
phenylsulfonic acid	PS-SiNP
long-chain alkylsulfonic acid	LS-SiNP

Successful functionalization of the SiNPs with the various surface chemistries was confirmed by using both FTIR and zeta-potential (ζ) measurements. The FTIR spectra for the different functionalizations were consistent with the literature[21,38,43−47] and can be found in the in the Supporting Information (see Figures S1 and S2). The results from zeta-potential experiments are shown in Table 2.

Table 2. Zeta-Potentials of Unfunctionalized and Functionalized Silica Nanoparticles Dispersed in Water under Acidic Conditions (pH ≈ 2)

SiNP functionality	zeta-potential (ζ) [mV]	SiNP functionality	zeta-potential (ζ) [mV]
UF-SiNP	−13.9[a]	TA-SiNP	+31.2[a]
AS-SiNP	−38.7	AA-SiNP	+23.7
PS-SiNP	−29.9[a]	PA-SiNP	+21.1
LS-SiNP	−41.5	LA-SiNP	+24.5

[a]Indicates previously published data.[20]

As it is difficult to determine the local pH that the SiNPs experience within the Nafion membranes when hydrated, the apparent pH of the Nafion solution (apparent pH of ≈2) can be taken to represent the average pH encountered by the SiNPs.[20] As such, all zeta-potential measurements were performed at a pH of ≈2. At these conditions, the hydroxyl groups on the surface the unmodified SiNPs are near their isoelectric point (the shift between deprotonated and protonated),[48] yielding a zeta-potential closer to zero (though still slightly anionic). For amine-functionalized NPs, a protonated (or cationic) surface is expected, yielding a positive zeta-potential, while SiNPs with sulfonic acid functionality should have a deprotonated (or anionic) surface, yielding a negative zeta-potential. The zeta-potentials for each of the specific functionalized NPs are shown in Table 2 and follow the expected trends.[48,49] In addition, nanoparticles with $\zeta \leq -30$ mV are considered to have highly anionic surfaces, while nanoparticles with $\zeta \geq +30$ mV are considered to have highly cationic surfaces.[50] Successful functionalization of each of the SiNPs is indicated by the change from a zeta-potential of −13.9 mV for the unfunctionalized particles,[20] where all of the amine-functionalized particles are moderately cationic (+21.1

DOI: 10.1021/acsaem.9b01443
ACS Appl. Energy Mater. 2019, 2, 8535−8549

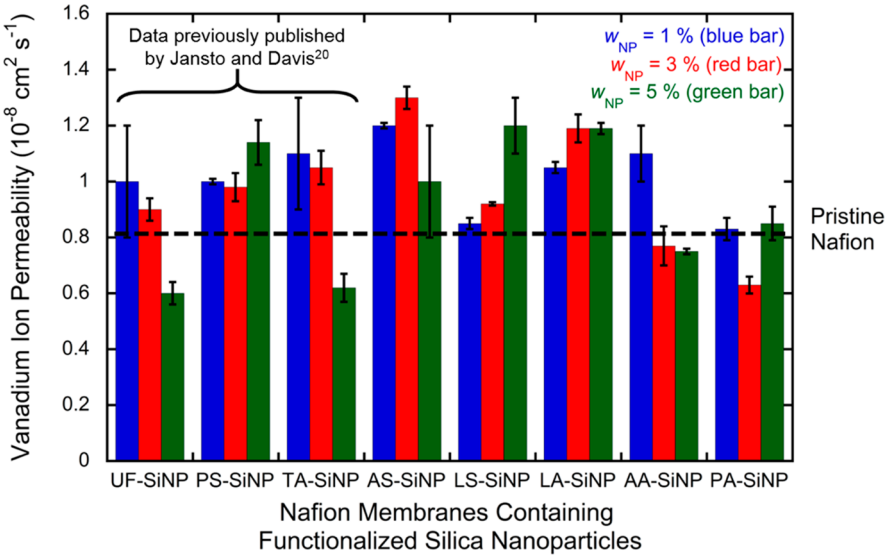

Figure 2. Vanadium ion permeability for Nafion membranes containing w_{NP} = 1% (dark blue bar), w_{NP} = 3% (red bar), and w_{NP} = 5% (green bar) SiNPs for each surface functionalization. The dashed horizontal black line and the first three groupings of bars labeled UF-SiNP, PS-SiNP, and TA-SiNP represent previously reported vanadium ion (VO^{2+}) permeabilities for pristine Nafion and Nafion containing UF-SiNP, PS-SiNP, and TA-SiNP.[20] Error bars represents the standard deviation of at least three repeat experiments.

to +31.2 mV) and the sulfonic acid-functionalized particles are all highly anionic (−41.5 to −29.9 mV).

Nanocomposite Membrane Permeability. Vanadium ion permeation experiments were performed on pristine Nafion (i.e., membranes containing no SiNPs) and Nafion−SiNP nanocomposite membranes containing SiNP at w_{NP} = 1%, w_{NP} = 3%, and w_{NP} = 5% (where w_{NP} is the mass fraction of NPs in Nafion, i.e., (mass of SiNPs/total mass of solids) × 100%). The results of the vanadium ion crossover experiments, for each surface functionalization, are shown in Figure 2. The dashed horizontal black line represents the average vanadium ion permeability for pristine Nafion membranes ((0.81 ± 0.05) × 10^{-8} cm^2 s^{-1}).[20] Additionally, the permeation values shown in first three groupings of columns, labeled UF-SiNP, PS-SiNP, and TA-SiNP, were previously published.[20] The error in these data represents the standard deviation of at least three repeat experiments. As seen in Figure 2, the vanadium ion permeability was, for the most part, consistently higher for membranes containing SiNPs at w_{NP} = 1% than that observed for pristine Nafion, ranging from 5% to 50%, regardless of the surface chemistry. These results are similar to those previously reported, where higher permeability was observed for ionomer membranes containing SiNPs at w_{NP} = 1%.[20] Notably, Nafion nanocomposites containing UF-SiNP and TA-SiNP at w_{NP} = 5% exhibited the highest reduction of vanadium ion permeability with respect to pristine Nafion.[20] To help parse out the influence of the electrosteric stabilizing factors introduced by the nanoparticle surface functionalization on the observed vanadium ion permeability, ion exchange capacity (IEC) and equilibrium acid uptake experiments were performed on each of the ionomer nanocomposite membranes (see Figures S3 and S4).

As seen in Figure 2, the introduction of sulfonic acid-functionalized SiNPs into the ionomer membrane increased the IEC with respect to the pristine Nafion membrane (by >10% for all SiNP loading of LS-SiNP and AS-SiNP; see Figure S3), indicating that additional sulfonic acid charges have been introduced into the membranes. The Donnan principle explains that positively charged vanadium ions (so-called "counterions" in this case) can experience a change in flux through the membrane as the number of fixed negative charges in the ionomer either decreases or increases.[51,52] We conjecture the increase in IEC observed for the introduction of sulfonic acid-functionalized SiNPs is caused by two factors: (1) additional number of charged sulfonic acid groups introduced with SiNPs, shifting the Donnan equilibrium and (2) sulfonic acid-functionalized SiNPs increase the connectivity of the ionic channels by altering the formation of ionic network as the solvent evaporates during membrane formation, increasing accessibility to sulfonic acid sites within Nafion that were previously inaccessible. Ultimately, this leads to an overall increased vanadium ion crossover through Nafion nanocomposites films with sulfonic acid-functionalized SiNPs, especially at higher SiNP loadings.

Also seen in Figure 2, the vanadium ion permeability of membranes containing AA-SiNP at w_{NP} = 3% and w_{NP} = 5% ((0.77 ± 0.07) × 10^{-8} cm^2 s^{-1} and (0.75 ± 0.01) × 10^{-8} cm^2 s^{-1}, respectively) were not significantly different than that of pristine Nafion, where only a ≈ 5% reduction was observed for membranes containing AA-SiNP at w_{NP} = 5%. From Figure S3, we see that the IEC values for membranes containing AA-SiNP at all SiNP loadings are similar to that of pristine Nafion, indicating that the number of fixed charges within the ionomer membrane is essentially the same between these membranes. This helps to explain the similar vanadium ion permeability. Compared to the membranes containing sulfonic acid-functionalized SiNPs, the introduction of amine-functionalized SiNPs into the ionomer membrane can shift the Donnan equilibrium to reduce vanadium ion flux in two ways: (1) the amine-functionalized SiNP may sequester the sulfonic acid pendant chains within the ionic domains of Nafion, and/or (2) free cations of the amine-functionalized SiNP (those not directly interacting with the sulfonic acid groups) may act as co-ions to the vanadium cations. A reduction in IEC demonstrates evidence of these phenomena. In this case, as the IEC for the membranes containing AA-SiNP at w_{NP} = 3%

DOI: 10.1021/acsaem.9b01443
ACS Appl. Energy Mater. 2019, 2, 8535−8549

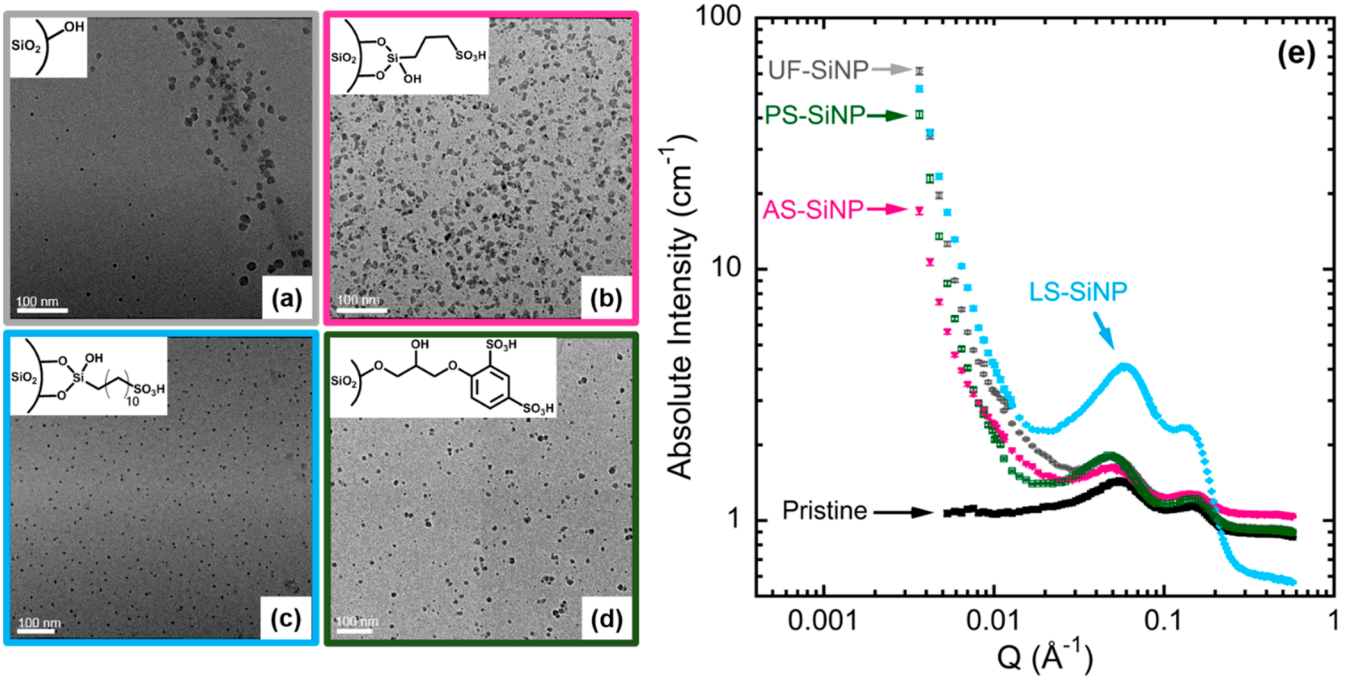

Figure 3. TEM images of Nafion−SiNP nanocomposite membranes containing (a) w_{NP} = 5% UF-SiNP, (b) w_{NP} = 5% AS-SiNP, (c) w_{NP} = 5% LS-SiNP, and (d) w_{NP} = 5% PS-SiNP. The scale bars for TEM images are all 100 nm. (e) SANS curves for Nafion and Nafion nanocomposites containing sulfonic acid-functionalized SiNPs at w_{NP} = 5%. All membranes were hydrated in 100% H_2O for at least 24 h prior to SANS experiments.

and w_{NP} = 5% is similar to that of pristine Nafion, it is no surprise these membranes demonstrate similar vanadium ion permeabilities to that of pristine Nafion.[20]

Membranes containing LA-SiNP at w_{NP} = 3% and w_{NP} = 5% demonstrated increased vanadium ion permeability ((1.19 ± 0.05) × 10^{-8} cm^2 s^{-1} and (1.19 ± 0.02) × 10^{-8} cm^2 s^{-1}, respectively), similar to the increase observed in membranes with sulfonic-acid functionalized SiNPs, which can be explained, in part, by variations in both the IEC (increased ≈15% with respect to pristine Nafion; see Figure S3) and the equilibrium acid uptake (increased by ≈50%; see Figure S4). The only membranes that exhibited reduced vanadium ion crossover were those containing PA-SiNP at w_{NP} = 3%, for which the crossover was reduced by ≈25%. As seen from Figure 2, this reduction in vanadium ion permeability was comparable to the reduction in permeability achieved by the introduction of UF-SiNP at w_{NP} = 5%. Results from IEC measurements on this membrane indicate a shift in the Donnan equilibrium of the system, leading to the rejection of a higher number of positively charged vanadium ions (IEC of membranes containing PA-SiNP at w_{NP} = 3% reduced by ≈10% compared to pristine Nafion; see Figure S3). This follows with previous results for Nafion membranes containing TA-SiNP at w_{NP} = 5% (see Figure 2), where an ≈25% reduction in vanadium ion permeability was observed. The reduction in vanadium ion permeability was, in part, a result of the lower IEC values measured for these membranes (see Figure S3). This decrease in IEC was expected as the number of amine groups per functional group on the surface was greatest for the TA-SiNPs.

However, membranes containing PA-SiNP at w_{NP} = 5% exhibited similar IEC values to those containing w_{NP} = 3% but demonstrated increased vanadium ion crossover. We postulate that this anomaly may be due to a combination of different factors, as the addition of more PA-SiNP may lead to (1) changes in the silica phase in the ionomer (i.e., changes in the dispersion state), (2) changes in the ionic domain formation (i.e., increased connectivity of the previously inaccessible sulfonic acid groups and creating a less tortuous path for the vanadium ions), and/or (3) changes to the segmental relaxation dynamics of the ionomer nanocomposite. While counterintuitive, increasing the loading of nanoparticles in these ionomer membranes does not necessarily lead to a decrease in segmental dynamics of the nanocomposite. Recent work from our group demonstrated that the introduction of more nanoparticles into the ionomer membrane (increase from w_{NP} ≈ 4% to w_{NP} ≈ 10%) led to an increase in the segmental relaxation dynamics of the nanocomposite.[53] These data will be discussed in further detail in the context of membrane morphology and nanoparticle dispersion state in the following section.

Nanocomposite Membrane Morphology. Nafion−SiNP nanocomposite morphology was investigated by using both TEM and SANS. The results from this analysis, for membranes containing UF-SiNP and sulfonic acid-functionalized SiNPs, are shown in Figure 3. Specifically, TEM images for Nafion membranes containing UF-SiNP, AS-SiNP, LS-SiNP, and PS-SiNP at w_{NP} = 5% are shown in Figure 3a−d, while SANS curves for pristine Nafion and Nafion containing negatively charged sulfonic acid-functionalized SiNPs at w_{NP} = 5% (hydrated in 100% H_2O) are shown in Figure 3e. In general, each of the TEM images indicates well-dispersed NPs, with diameters ranging from (5−15) nm, which is consistent with the as-received SiNPs (see the Experimental Section). Note that while the scale bars in each TEM image are 100 nm in length, the exact magnification for all TEM images varies between 25000× and 40000×. The TEM images of Nafion containing sulfonic acid-functionalized NPs (AS-SiNP, LS-SiNP, and PS-SiNP in Figures 3b−d, respectively) indicate that the particles are well dispersed, with only a few aggregates on

DOI: 10.1021/acsaem.9b01443
ACS Appl. Energy Mater. 2019, 2, 8535−8549

Table 3. SANS Peak Positions and Power Law Fitting of Low-Q Region for Pristine Nafion and Nafion Nanocomposite Membranes Containing SiNPs at w_{NP} = 5%

	crystalline		ionomer		low Q
functionalization	peak position [Å^{-1}]	d-spacing [nm]	peak position [Å^{-1}]	d-spacing [nm]	power law exponent α
no SiNPs					
pristine Nafion	0.0584	10.8	0.141	4.45	
no functionalization					
UF-SiNP	0.0517	12.2	0.141	4.45	3.27
sulfonic acid					
AS-SiNP	0.0504	12.5	0.141	4.45	3.32
PS-SiNP	0.0490	12.8	0.152	4.14	4.32
LS-SiNP	0.0598	10.5	0.146	4.29	3.37
amine					
TA-SiNP	0.0450	14.0	0.141	4.45	3.84
AA-SiNP	0.0517	12.2	0.141	4.45	3.57
PA-SiNP	0.0490	12.8	0.141	4.45	
LA-SiNP	0.0450	14.0	0.141	4.45	4.07

the order of <5 particles. Notably, the most uniform dispersion was observed for nanoparticles functionalized with the longest alkyl chain (LS-SiNP, 11-carbon chain), where no aggregation or clustering of NPs was observed in the TEM images. This follows the expected dispersion behavior predicted by DLVO theory, where increasing the length of grafted chains prevents crowding of nanoparticles, leading to a more homogeneous distribution of nanoparticles within the membrane.[27] Unlike the sulfonic acid-functionalized SiNPs, membranes containing UF-SiNP at w_{NP} = 5% (see Figure 3a) exhibit diffuse clustering of NPs that span several hundreds of nanometers across the image; however, there are no large nanoparticle aggregates in any of the TEM images shown in Figure 3. Here, the term "diffuse" refers to NPs that are loosely grouped together but are not necessarily touching each other.

To complement the real-space images taken by TEM, SANS experiments were performed on Nafion and Nafion nanocomposite films (hydrated in 100% H_2O), and the results of these measurements are shown in Figure 3e. While the exact nanophase-segregated morphology of Nafion has been debated for decades,[1,7,17] one of the most supported theories suggests the presence of interconnected pathways of spherical ionic clusters, surrounded by the mechanically robust hydrophobic backbone, known as the cluster-network model.[1] The SANS curve for pristine Nafion contains two prominent scattering peaks. The scattering peak at low Q ($Q \approx 0.058$ Å^{-1}) can be assigned to spacing between crystalline domains in the hydrophobic region of Nafion, while the scattering peak at high Q ($Q \approx 0.14$ Å^{-1}) is attributed to the spacing between the sulfonic acid groups in the hydrophilic, ionic domain of Nafion.[3] The values for the low-Q and high-Q peaks correspond to real-space values of ≈10.8 and ≈4.45 nm, respectively. Additionally, the SANS curves for Nafion nanocomposite membranes shown in Figure 3e exhibit these same two scattering peaks. The Q-spacing and corresponding real-space values for pristine Nafion and Nafion nanocomposites are summarized in Table 3.

In contrast to the SANS curve for pristine Nafion, the SANS curves for each of the nanocomposites exhibit a sharp low-Q upturn (starting around $Q \approx 0.03$ Å^{-1}), indicating the presence of larger structures >20 nm within the nanocomposites. For polymer nanocomposites, this sharp low-Q upturn is traditionally attributed to NP aggregation.[23] It is important to note that while the exact number and shape/tortuosity of interconnected ionic pathways within Nafion may change slightly by the addition of NPs (as evidenced by IEC measurements),[54] NPs that are significantly larger than ≈5 nm are unlikely to distort the ionic domains enough to allow for the NPs to fully reside within these ionic pathways, leading to NP aggregation. However, as seen from the TEM images, there is no significant aggregation observed for Nafion membranes containing either UF-SiNP or sulfonic-acid functionalized SiNPs. It is worth noting that the TEM images shown in Figure 3a–d are only (0.3–0.7) μm^2 in size, and these drop-cast membranes are <100 nm thick (see the Experimental Section). These specific images have been selected as they are representative of the overwhelming majority of TEM images captured during this analysis; however, it is possible that larger aggregates and/or more diffuse clusters are present in the bulk films, which were used in the SANS measurements and have thicknesses of ≈50 μm.

With the exception of membranes containing LS-SiNPs, which showed negligible changes in d-spacing, the introduction of UF-SiNP, AS-SiNP, and PS-SiNP, on average, increased the d-spacing of crystalline domains within the hydrophobic region by ≈15% (see Table 3). Similarly, the location of the scattering peak associated with the ionic (hydrophilic) domain does not significantly change when compared to pristine Nafion (see Table 3), though we do see a slight reduction in the d-spacing for membranes containing PS-SiNP (≈10% reduction) and LS-SiNP (≈5% reduction). As the formation of interconnected ionic channels is paramount for facile transport, changes to the hydrated, ionic structure of the membrane could lead to changes in the resultant transport properties of the ionomer nanocomposite membranes.[55] Interestingly, this result indicates that the overall ionic network structure is not drastically altered by the introduction of the SiNPs, at least within the sensitivity of the SANS experiments. However, we know that changes to the chemical functionality of the ionic network within the membrane have occurred due to the measured differences in IEC and equilibrium acid uptake of the nanocomposite membranes when compared to pristine Nafion (see Figures S3 and S4). This result suggests that the mechanism by which vanadium ion crossover is reduced in these membranes is more complex than the simple steric hindrance mechanism previously proposed.[3,20,53]

This analysis was extended to Nafion membranes containing positively charged, amine-functionalized SiNPs, and the results

DOI: 10.1021/acsaem.9b01443
ACS Appl. Energy Mater. 2019, 2, 8535–8549

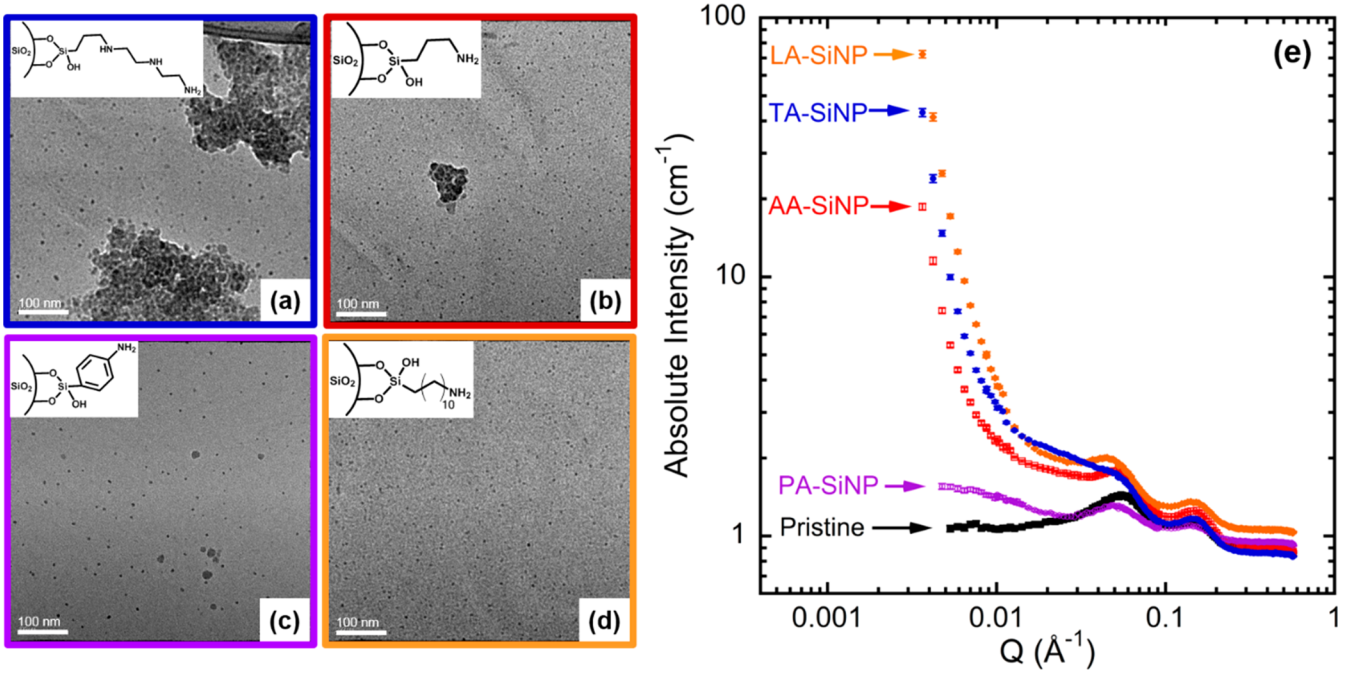

Figure 4. TEM images of Nafion−SiNP nanocomposite membranes containing (a) w_{NP} = 5% TA-SiNP, (b) w_{NP} = 5% AA-SiNP, (c) w_{NP} = 5% PA-SiNP, and (d) w_{NP} = 5% LA-SiNP. Scale bars for TEM images are all 100 nm. (e) SANS curves for Nafion and Nafion nanocomposites containing amine-functionalized SiNPs at w_{NP} = 5%. All membranes were hydrated in 100% H_2O for at least 24 h prior to SANS experiments.

from this analysis are shown in Figure 4. Specifically, TEM images for Nafion membranes containing TA-SiNP, AA-SiNP, PA-SiNP, and LA-SiNP at w_{NP} = 5% are shown in Figures 4a−d, respectively, while SANS curves for pristine Nafion and Nafion containing amine-functionalized SiNPs at w_{NP} = 5% (hydrated in 100% H_2O) are shown in Figure 4e. When compared with the TEM images for membranes containing sulfonic acid-functionalized SiNPs, the dispersion state of the amine-functionalized SiNPs within the ionomer membrane is drastically different. Most noticeably, significant aggregation was observed for two of the four amine surface functionalizations (TA-SiNP and AA-SiNP). Specifically, aggregates on the order of hundreds of nanometers were observed for both surface functionalizations, with the largest aggregates observed for Nafion membranes containing TA-SiNP. In contrast, Nafion membranes containing LA-SiNP and PA-SiNP exhibited excellent dispersion. The homogeneous dispersion of LA-SiNPs in the ionomer is again attributed to long alkyl chain (11-carbon chain) grafted onto the surface of the nanoparticles.[27] The excellent dispersion of the PA-SiNPs within the Nafion may be attributed to the phenyl rings contained in the bridging chain. Reduced aggregation has been previously observed for similar surface functionalized nanoparticles (series of nanoparticles grafted with phenyl-containing ligands)[56] and was attributed to the protection provided by the bulky phenyl rings on the surface of the nanoparticles.

The presence of large SiNP aggregates in membranes containing TA-SiNP and AA-SiNP (as observed in the TEM images) was corroborated by SANS studies on these membranes. Similar to the SANS curves for membranes containing sulfonic acid-functionalized SiNPs (see Figure 3e), the SANS curves shown in Figure 4e exhibit a sharp low-Q upturn, indicative of the presence of larger scattering structures (i.e., NP aggregates). Surprisingly, a sharp low-Q upturn was observed for Nafion membranes containing LA-SiNP, which seems to contradict the real-space images obtained via TEM. As we noted with the sulfonic acid-functionalized nanoparticles, while we did not observe any significant aggregation in any of the TEM images collected on these particular membranes, we cannot exclude the possibility of larger aggregates of LA-SiNPs in these nanocomposite membranes. In contrast to all other amine-functionalized nanoparticles, only a slight upturn in the low-Q data is observed for Nafion containing PA-SiNPs. This result follows with the TEM images obtained for these membranes.

Compared to the changes in d-spacing of hydrophobic domains observed for membranes containing sulfonic acid-functionalized SiNPs, the introduction of amine-functionalized SiNPs into the ionomer resulted in more pronounced changes to the d-spacing of the crystalline domains within the hydrophobic region of the resultant nanocomposite membrane, ranging from approximately 15% to 30% increase in d-spacing for all amine-functionalized SiNPs compared to pristine Nafion. For example, the low-Q peak shifts to lower Q values for membranes containing TA-SiNP and LA-SiNP, increasing from a d-spacing of (10.8−14.0) nm when compared to pristine Nafion, an approximate 30% increase. This shift to lower Q values was observed in nearly all nanocomposite samples, with only membranes containing LS-SiNP exhibit a slight decrease in crystalline spacing (from 10.8 nm to 10.5 nm). These results indicate that the introduction of SiNPs into the membrane has, on average, a more significant impact on the hydrophobic domain of Nafion, while their impact on the spacing of the ionic domains is minimal.

To elucidate how nanoparticle loading impacts the low-Q upturn observed in the SANS curves, SANS experiments on Nafion membranes containing UF-SiNP, PS-SiNP, and TA-SiNP, at various nanoparticle loadings, were performed. These three surface chemistries were selected as representative

DOI: 10.1021/acsaem.9b01443
ACS Appl. Energy Mater. 2019, 2, 8535−8549

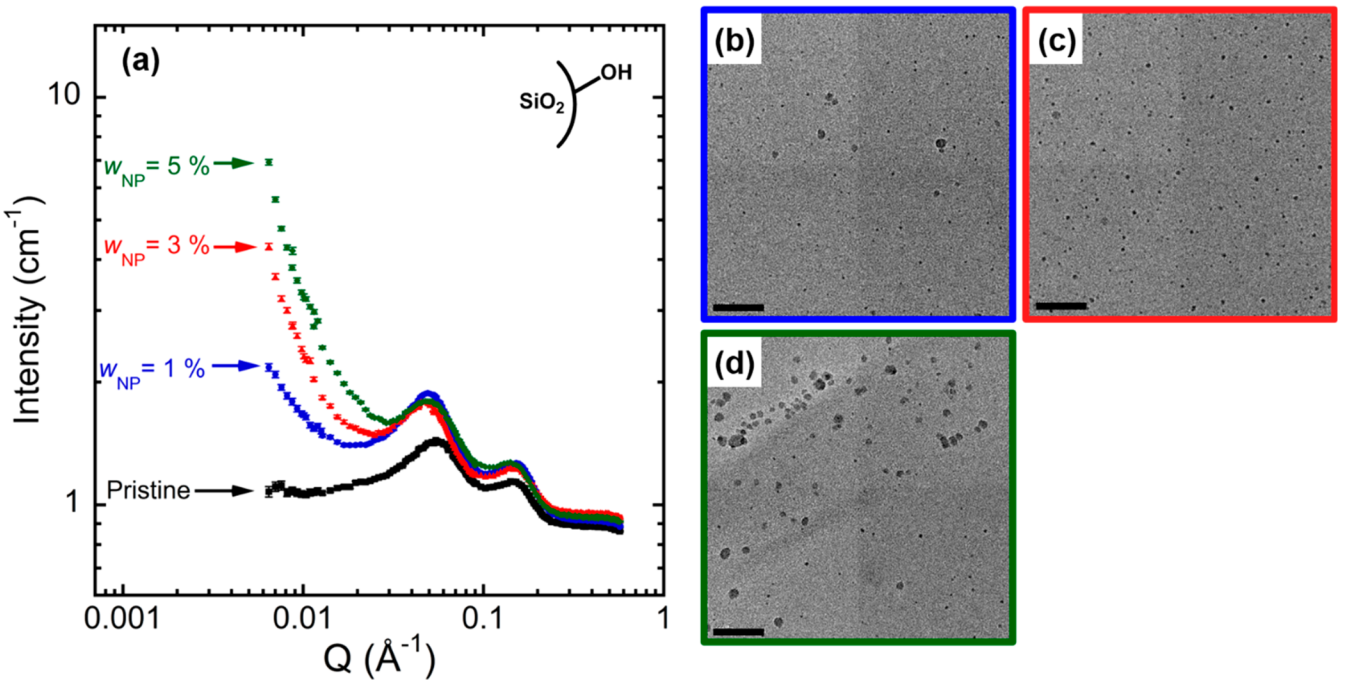

Figure 5. (a) SANS curves for Nafion−SiNP nanocomposite membranes containing w_{NP} = 0% (pristine Nafion; closed black squares), w_{NP} = 1% (closed blue circles), w_{NP} = 3% (closed red triangles), and w_{NP} = 5% (closed green diamonds) UF-SiNP. All membranes were hydrated in 100% H_2O for at least 24 h prior to SANS experiments. TEM images of Nafion−SiNP nanocomposite membranes containing (b) w_{NP} = 1%, (c) w_{NP} = 3%, and (d) w_{NP} = 5% UF-SiNP. The scale bars for all TEM images are 100 nm. TEM images adapted with permission from ref 20.

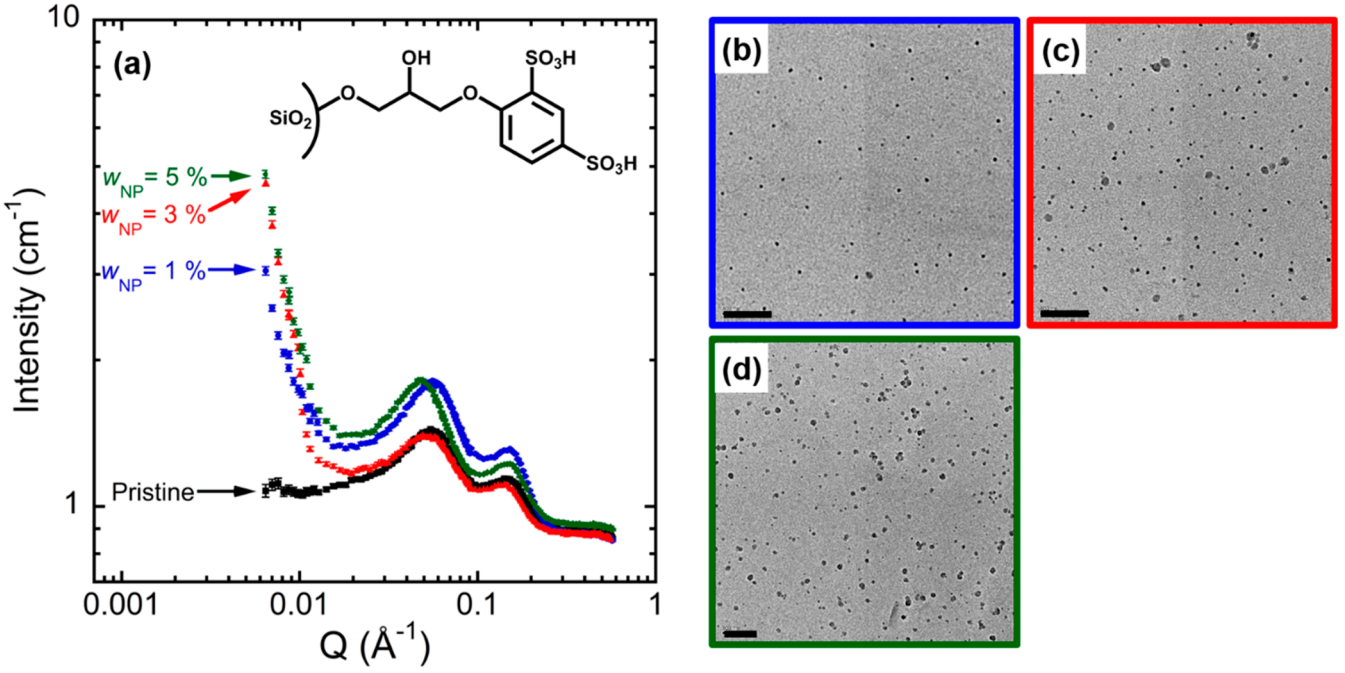

Figure 6. (a) SANS curves for Nafion−SiNP nanocomposite membranes containing w_{NP} = 0% (pristine Nafion; closed black squares), w_{NP} = 1% (closed blue circles), w_{NP} = 3% (closed red triangles), and w_{NP} = 5% (closed green diamonds) PS-SiNP. All membranes were hydrated in 100% H_2O for at least 24 h prior to SANS experiments. TEM images of Nafion−SiNP nanocomposite membranes containing (b) w_{NP} = 1%, (c) w_{NP} = 3%, and (d) w_{NP} = 5% PS-SiNP. The scale bars for all TEM images are 100 nm. TEM images adapted with permission from ref 20.

functionalization for each category: unfunctionalized, sulfonic acid-functionalized, and amine-functionalized. Figure 5 shows the SANS curves for Nafion−SiNP nanocomposites with UF-SiNP at w_{NP} = 1%, w_{NP} = 3%, and w_{NP} = 5% (hydrated in 100% H_2O). Also included in Figure 5 are the TEM images corresponding to the SANS curves at each SiNP loading. As seen from Figure 5, the SiNP dispersion states observed in the real-space TEM images correspond nicely with upturn at lower Q values in the SANS data. For example, the TEM images for Nafion membranes containing UF-SiNP at w_{NP} = 1%, w_{NP} = 3%, and w_{NP} = 5% (Figures 5b, 5c, and 5d, respectively) show an increase in the concentration of diffuse NP clusters as the

DOI: 10.1021/acsaem.9b01443
ACS Appl. Energy Mater. 2019, 2, 8535−8549

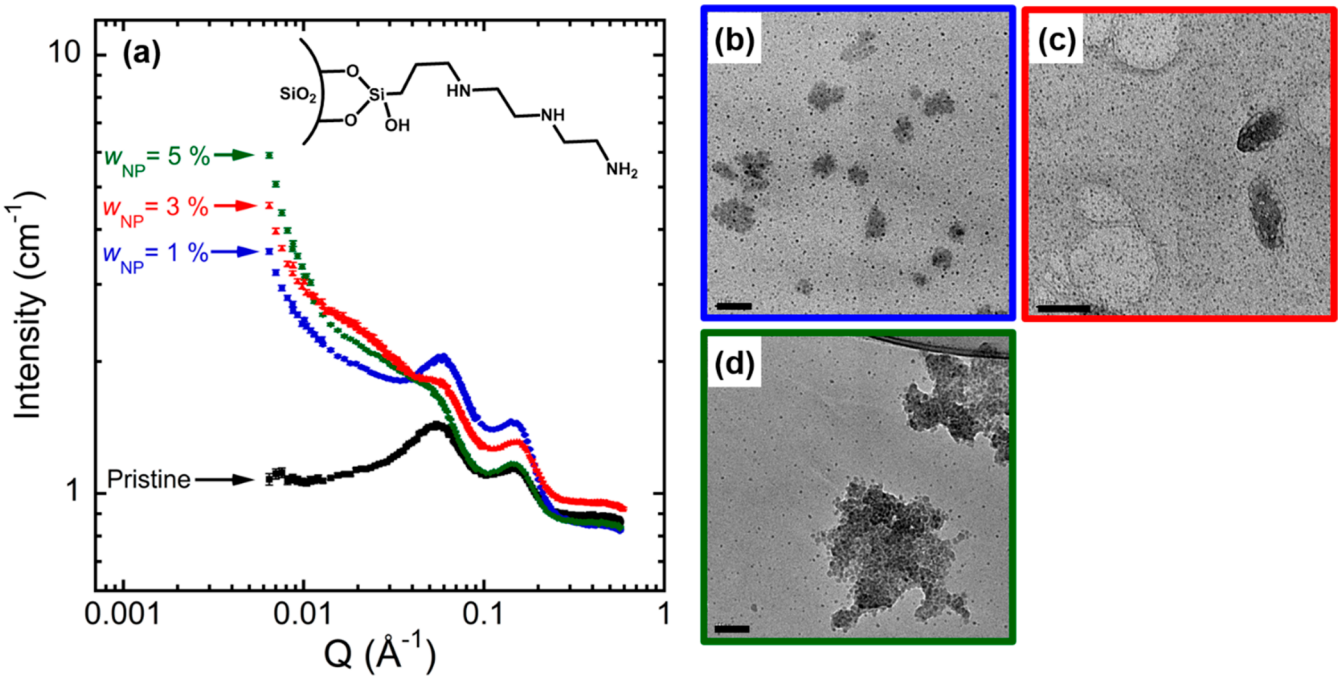

Figure 7. (a) SANS curves for Nafion−SiNP nanocomposite membranes containing w_{NP} = 0% (pristine Nafion; closed black squares), w_{NP} = 1% (closed blue circles), w_{NP} = 3% (closed red triangles), and w_{NP} = 5% (closed green diamonds) TA-SiNP. All membranes were hydrated in 100% H_2O for at least 24 h prior to SANS experiments. TEM images of Nafion−SiNP nanocomposite membranes containing (b) w_{NP} = 1%, (c) w_{NP} = 3%, and (d) w_{NP} = 5% TA-SiNP. The scale bars for all TEM images are 100 nm. The w_{NP} = 5% TA-SiNP TEM image (d) was adapted with permission from ref 20.

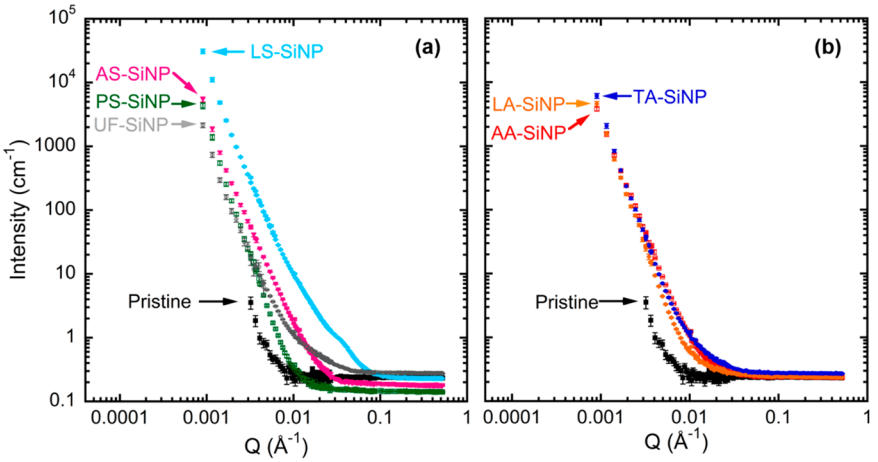

Figure 8. Contrast-match SANS curves for pristine Nafion and Nafion−SiNP nanocomposite membranes containing (a) sulfonic acid-functionalized SiNPs and (b) amine-functionalized SiNPs at w_{NP} = 5%. All membranes were soaked in a 24:76 mixture (by volume) of H_2O:D_2O for at least 24 h prior to SANS experiments.

mass fraction of SiNPs is increased. The increase in the concentration of theses clusters, as the NP loading is increased from w_{NP} = 1% to w_{NP} = 5%, is indirectly captured by the increase in intensity of the low-Q SANS data (moving from the filled blue circles to the filled green diamonds in Figure 5a).

Figure 6 shows the SANS curves for Nafion−SiNP nanocomposites with PS-SiNP at w_{NP} = 1%, w_{NP} = 3%, and w_{NP} = 5% (hydrated in 100% H_2O). Also included in Figure 6 are the TEM images corresponding to the SANS curves at each SiNP loading. As seen in Figure 6, the increasing PS-SiNP loading does little to affect either the SANS curves (Figure 6a) or the PS-SiNP dispersion state (Figures 6b−d). However, the *d*-spacing between the crystalline domains shifts slightly with higher mass fraction PS-SiNP, most evident between the curves for the membranes containing w_{NP} = 1% (blue) and w_{NP} = 5% (green) PS-SiNP in Figure 6a.

Figure 7 shows the SANS curves for Nafion−SiNP nanocomposites with TA-SiNP at w_{NP} = 1%, w_{NP} = 3%, and w_{NP} = 5% (hydrated in 100% H_2O). Also included in Figure 7 are the TEM images corresponding to the SANS curves at each SiNP loading for TA-SiNP. In contrast to what is observed in Figure 5a, the low-Q upturn seen in Figure 7a for Nafion membranes containing TA-SiNP does not significantly change as the NP loading is increased from w_{NP} = 1% to w_{NP} = 5% (moving from the filled blue circles to the filled green diamonds in Figure 7a), providing in indirect indication that

DOI: 10.1021/acsaem.9b01443
ACS Appl. Energy Mater. 2019, 2, 8535−8549

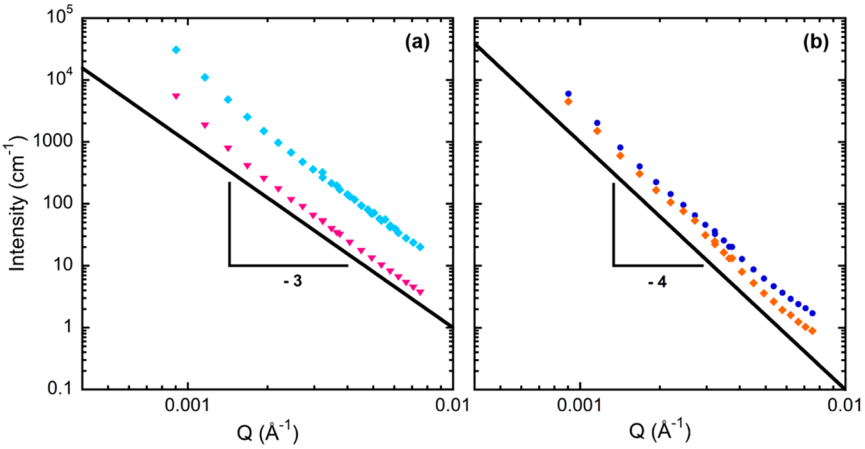

Figure 9. Corrected low-Q SANS data of Nafion membranes containing (a) sulfonic acid-functionalized SiNPs, LS-SiNP (closed light blue diamonds) and AS-SiNP (closed pink triangles), at w_{NP} = 5% and (b) amine-functionalized SiNPs, TA-SiNP (closed dark blue circles) and LA-SiNP (closed orange diamonds), at w_{NP} = 5%. The black lines within each figure are drawn with the appropriate power law exponent to guide the reader's eye.

the concentration of NP aggregates does not appreciably change with NP loading. This is confirmed by the corresponding real-space TEM images for membranes containing TA-SiNP at w_{NP} = 1%, w_{NP} = 3%, and w_{NP} = 5%, which are shown in Figures 7b, 7c, and 7d, respectively. The TEM images reveal the presence of large (>100 nm in diameter) NP aggregates at all loadings. Combining the findings from SANS, TEM, and IEC experiments, as well as previous thermomechanical studies,[57] we conjecture that the NP aggregates either reside in this hydrophobic region or at the boundary of the hydrophobic and hydrophilic domains (or some combination of both). These results seem to indicate that the addition of SiNPs to Nafion does not affect vanadium ion crossover by sterically impeding ion transport in the ionic domains, as per the mechanism previously hypothesized.[8,18] Instead, we believe the introduction of the SiNPs acts to alter vanadium ion transport through a combined mechanism, which includes (1) altering the available sulfonic acid groups available for vanadium ion transport and (2) altering the ionomer chain dynamics, where the latter has been observed in recent neutron spin echo spectroscopy studies on these ionomer nanocomposites.[53]

To gain additional insight into the structure of the inorganic NP phase within the nanocomposite membrane, a series of contrast-match SANS experiments were conducted. For these experiments, the nanocomposite films (at w_{NP} = 5%) were hydrated in a solution of H_2O and D_2O (24:76 by volume H_2O:D_2O). Based on the scattering length density (SLD) of H_2O (SLD = -0.5×10^{-6} Å^{-2})[58] and D_2O (SLD = 6.4×10^{-6} Å^{-2}),[58] a solvent environment with a scattering length density (SLD) of ≈4.7×10^{-10} cm^{-2} was created.[3] This value is comparable to that of Nafion (SLD ≈ 4.5×10^{-10} cm^{-2}; based on chemical formula),[59] thus reducing the scattering contrast of Nafion in the system to zero. That is, the SLD of the solvent has been chosen so that any measured scattering can be attributed to the silica phase within the nanocomposite membrane.[3]

Surprisingly, as seen in Figure 8, the SANS curve for pristine Nafion shows a low-Q upturn that was not previously observed in the SANS data for membranes hydrated in 100% H_2O. A similar upturn has been previously observed for extruded Nafion membranes (Nafion 112, Nafion 115, and Nafion 117) with high degrees of crystallinity (hydrated in 100% H_2O).[60−62] Previous contrast-match experiments performed by our group (for both extruded and solution-cast Nafion membranes) were performed on the NG-B 10 m SANS beamline at the NCNR,[3] and thus the upturn was not evident, given the range of Q values explored. At present, adequate experiments have not been conducted to accurately elucidate what structural features give rise to this low-Q upturn observed in the SANS data. However, it is apparent that these larger structural features have a comparable SLD to that of H_2O, resulting in the low-Q upturn only being observable when the membranes were hydrated in a solution of H_2O and D_2O.[59] Note, the Q range for the pristine Nafion data shown in Figure 8 is smaller than the Q range of the nanocomposite membranes as SANS data for this membrane were collected on a different SANS instrument (see the Experimental Section).

Under contrast-match hydration, the membranes containing sulfonic acid-functionalized SiNP (LS, AS, and PS) have different scattering patterns, in both the low-Q and mid-Q regions. As seen in Figures 8a,b, apart from the low-Q upturn, there are no features observed in scattering data of the nanocomposites, except those containing LS-SiNP. This suggests that the functionalizations on the surface of the SiNPs do not self-assemble to form any long-range order. In the case of membranes containing LS-SiNP, the slight shoulder observed in the mid-Q region could arise from (1) an additional structural feature present for these nanocomposite membranes or (2) the representative scattering peak for the crystalline spacing has shifted to lower Q values and is no longer contrast-matched out by the H_2O:D_2O solution. In addition, as seen in Figure 8a, the low-Q upturn in SANS data for membranes containing LS-SiNP begins at higher Q values, i.e., smaller length scale ($Q \approx 0.06$ Å^{-1}, d-spacing ≈ 10 nm), with a shoulder at approximately the same location as would be expected for the crystalline peak of the Nafion. Compared to other sulfonic acid-functionalized SiNPs, the steepest slope in the low-Q data is observed for membranes containing PS-SiNP, with the low-Q upturn starting at the largest length scale ($Q \approx 0.01$ Å^{-1}, d-spacing ≈ 63 nm). Conversely, the contrast-match SANS data for membranes containing amine-functionalized SiNPs were all similar (Figure 8b), indicating the characteristic length scale of the silica aggregates in these

DOI: 10.1021/acsaem.9b01443
ACS Appl. Energy Mater. 2019, 2, 8535−8549

nanocomposites was similar across all surface functionalizations. Note that, under contrast-match conditions, the low-Q data for membranes containing PA-SiNP had high uncertainty; therefore, these data were excluded from Figure 8b and from further analysis.

From permeation and IEC data, we know that the formation of the ionic domains is highly dependent on the interactions between the silica phase and Nafion. However, the low-Q upturn of the pristine Nafion data renders it difficult to make any direct conclusions about the structure of the silica phase within the nanocomposite membrane. As such, the contrast-match SANS data for membranes containing nanoparticles must be deconvoluted. That is, prior to analyzing the low-Q data of the nanocomposites, scattering from the pristine Nafion must be removed. By removing the effect of the Nafion on the measured scattering data, we can obtain a more accurate picture of how the surface chemistry impacts the silica phase within these ionomer nanocomposites. Therefore, the low-Q data for pristine Nafion, and subsequently all nanocomposite membranes, were fit to the following power law equation

$$I(Q) = (\text{scale})Q^{-\alpha} + \text{background} \quad (2)$$

where the scale (source intensity) and α (power law exponent) were unitless fitting parameters for each membrane, and the background was set to zero. Next, the low-Q data for the nanocomposite films were corrected by subtracting the data for pristine Nafion from the absolute intensity of the low-Q data for the nanocomposite membranes. Finally, the corrected SANS data were fit to eq 2, and the exponents obtained for each nanocomposite are noted in Table 3. Additionally, the corrected low-Q data, ranging from approximately (0.0009−0.008) $Å^{-1}$, for membranes containing sulfonic acid- and amine-functionalized SiNPs are shown in Figures 9a and 9b, respectively.

As seen from Table 3, the power law exponents for the nanocomposite membranes fall within the range of three to four, which is indicative of surface fractal scattering. Specifically, $\alpha \approx 3$ indicates scattering due to "rough" surfaces, while $\alpha \approx 4$ indicates Porod-like scattering of "smooth" surfaces.[63,64] From this power law exponent, a fractal dimension, D_f, can also be ascertained, where $D_f = 6 - \alpha$ is a unitless ratio that describes geometrical complexity. More specifically, the surface fractal dimension $(2 \leq D_f \leq 3)$[63] elucidates the surface complexity, where $D_f = 2$ suggests a perfectly smooth surface and $D_f = 3$ suggests that the surface is so folded that it almost completely fills the space.[64] The power law exponents, after subtraction, for each nanocomposite membrane are shown in Table 3. As seen in Table 3, the power law exponent of the membranes containing PS-SiNP was higher than any other membrane and close to a value of 4, which is indicative of Porod-like scattering from sharp interfaces between phases.[64] In contrast, membranes containing LS-SiNP, AS-SiNP, and UF-SiNP have power law exponents closer to three. This result suggests that, with the exception of membranes containing PS-SiNP, a rough interface exists between the ionomer and anionic surface of the unfunctionalized and sulfonic acid-functionalized SiNPs. That is, these lower power law exponents indicate that the interface between the Nafion and silica phases is more "jagged" as compared to the Porod-like scattering observed in membranes containing PS-SiNPs.

The lack of clarity between phases is likely due to the diffuse clustering and other loosely joined aggregates observed in these membranes,[20] which one could imagine would have significantly larger surface areas as compared to tightly bound aggregates, i.e., a much rougher surface. The diffuse clustering of SiNPs may affect the nanocomposite morphology differently for the different surface functionalities, either increasing the ionic domain connectivity or otherwise affecting the chain dynamics.[53] Previous results from our group demonstrated that the introduction of UF-SiNP at $w_{NP} \approx 4\%$ resulted in a significant decrease in both the segmental and swelling dynamics, measured by neutron spin echo and FTIR spectroscopy, respectively, of the nanocomposite as compared to pristine Nafion.

For the sulfonic acid-functionalized SiNPs, we conjecture that an increased connectivity due to large diffuse clusters (supported by the IEC measurements; see Figure S3), in combination with the shifted Donnan equilibrium, leads to an increase in vanadium ion crossover as compared to pristine Nafion. For the UF-SiNP nanocomposite membranes, which demonstrated the highest reduction in vanadium ion permeability, the diffuse aggregates likely increase the tortuosity for the ionic domains and further sequester the sulfonic acid-capped pendant chains of Nafion, ultimately leading to a reduction in vanadium ion crossover. In both of these cases though, the SiNP dispersion state alone does not determine the transport properties of the membranes. Rather, it is a combination of SiNP dispersion state and SiNP surface charge that ultimately alters the morphology and ion transport through the ionomer.

In contrast to membranes containing sulfonic acid-functionalized SiNPs, we observed that the power law exponents for nanocomposites containing amine-functionalized SiNPs at $w_{NP} = 5\%$ (AA-SiNP, LA-SiNP, and TA-SiNP) were all above 3.5, with exponents ranging from 3.57 to 4.07. As mentioned above, power law exponents in this range are indicative of fractal nature of the NP surface, where fractal surfaces with $\alpha = 4$ (fractal dimension $D_f = 2$) are characterized by a smooth surface. Additionally, this Porod-like scattering is representative of sharp interfaces between phases.[64] These results indicate that a more well-defined interface between the SiNPs and the ionomer exists for membranes containing SiNPs with positively charged surfaces. The sharper interface between the amine-functionalized SiNPs and Nafion may affect the formation of the ionic domains within the nanocomposite membranes in different ways. As evidenced by the increased IEC for membranes containing LA-SiNP at all NP loadings (see Figure S3), the amine functionality may increase the connectivity of the ionic domains through interactions with the long bridging chain of the LA-SiNP, ultimately leading to accelerated vanadium ion crossover at all NP loadings. Alternatively, for membranes containing TA-SiNPs, the sharp interface of the large NP aggregates may increase the tortuosity (i.e., reduced connectivity) of the ionic domains, as evidenced by the reduced IEC value at $w_{NP} = 5\%$. Note that the largest reduction in vanadium ion permeability, as compared to pristine Nafion, was observed for membranes containing TA-SiNP at $w_{NP} = 5\%$, which was comparable to the reduction observed for membranes containing UF-SiNP at $w_{NP} = 5\%$ (shown in Figure 2). In addition to shifting the Donnan equilibrium, the presence of these larger aggregates likely results in a change in the conformational entropy of the local chains (i.e., morphology) of Nafion, impacting the local segmental relaxation dynamics, which are closely coupled to transport.[53,65−67] However, to date, the necessary spectroscopy

DOI: 10.1021/acsaem.9b01443
ACS Appl. Energy Mater. 2019, 2, 8535−8549

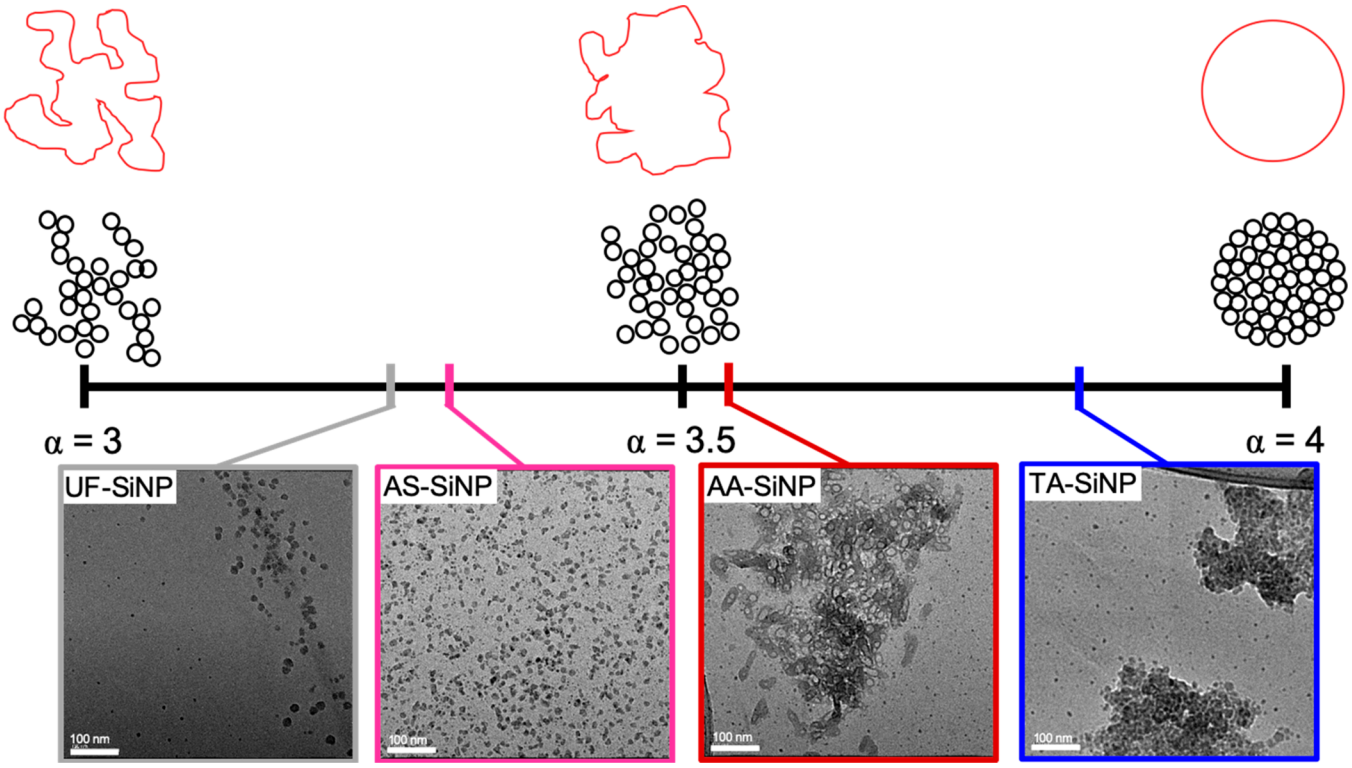

Figure 10. Illustrative schematic of surface fractal structure of SiNP aggregates as a function of the power law exponent obtained from SANS, with accompanying real-space TEM images of Nafion membranes containing UF-SiNP, AS-SiNP, AA-SiNP, and TA-SiNP (from L to R) at w_{NP} = 5%. The scale bars for TEM images are all 100 nm. The black circles represent the SiNP aggregates, while the red shape above these black circles is a representative outline of the aggregates, illustrating decreasing surface area of the aggregates as roughness decreases (going from α = 3 to α = 4).

experiments have not been performed on ionomer membranes containing TA-SiNPs, though these experiments are part of the scope of our future studies.

To further illustrate the correlation between the power law exponents extracted from analysis of the low-Q contrast-match SANS data and the corresponding real-space TEM images, an illustrative schematic depicting this relationship is shown in Figure 10. Specifically, Figure 10 shows where various Nafion–SiNP nanocomposites (at w_{NP} = 5%) lie along the power law exponent scale ($3 \leq \alpha \leq 4$), where the fractal surface roughness of the SiNP aggregates decreases as the power law exponent increases from three to four. The illustration of SiNPs shown as black circles (above the TEM images) depicts the decreasing surface roughness as the aggregates become more sphere-like, while the red outlines (above the black circles) show the decreasing surface area of the aggregates as the power law exponent increases from three to four. The representative TEM images demonstrate the change in aggregation from diffuse clusters (UF-SiNP and AS-SiNP) to larger and more abundant aggregates (AA-SiNP and TA-SiNP).

CONCLUSIONS

The incorporation of silica nanoparticles with various functionalities into Nafion membranes for use in VRFBs was seen to impact the vanadium ion crossover and membrane morphology compared to pristine Nafion membranes. The vanadium ion crossover increased for all of the Nafion nanocomposite membranes with sulfonic acid-functionalized nanoparticles, in part due to shifting the Donnan equilibrium (as evidenced by the IEC). Alternatively, the vanadium ion crossover also increased for several of the membranes with amine-functionalized nanoparticles, which we attributed to a combination of nanoparticle dispersion and nanocomposite morphology. Depending on the nanoparticle functionality, including both end-functionality and bridging group, the nanoparticle dispersion within Nafion membranes varied, ranging from well-dispersed particles (PS-SiNP, LS-SiNP, and LA-SiNP) to diffuse cluster-like aggregates (UF-SiNP and AS-SiNP) to larger, more abundant aggregates (TA-SiNP and AA-SiNP). The nanoparticle aggregation or dispersion is supported by both TEM images and SANS scattering, where the formation of the ionic domain has not been significantly altered for any of the nanocomposite membranes. To isolate the effect of the silica nanoparticle aggregates in each of the nanocomposite membranes, contrast-match SANS was utilized. The low-Q SANS region fit with a power law model yields fractal scattering for each of the functionalizations ranging from the diffuse clustering of the UF-SiNP, demonstrating a power law exponent of 3.27, to the densely packed and large aggregates of TA-SiNP, demonstrating a power law exponent of 3.84. Overall, the reduction in vanadium ion permeability due to the incorporation of SiNPs was found to occur as a result of the combination of perturbations to the local morphology, fixed ionic activity within the ionomer (Donnan principle), and perturbations to the SiNP dispersion state. Results from this work demonstrate how perturbations to this dispersion state can be directly tuned by manipulating the surface chemistry of the nanoparticles, resulting in changes to in nanoparticle–ionomer interactions.

DOI: 10.1021/acsaem.9b01443
ACS Appl. Energy Mater. 2019, 2, 8535–8549

■ ASSOCIATED CONTENT

Supporting Information

The Supporting Information is available free of charge at https://pubs.acs.org/doi/10.1021/acsaem.9b01443.

FTIR spectra of functionalized silica nanoparticles, ion exchange capacity measurements, and equilibrium acid uptake measurements (PDF)

■ AUTHOR INFORMATION

Corresponding Author

*E-mail ericd@clemson.edu.

ORCID

Allison Domhoff: 0000-0002-0264-0410
Apoorv Balwani: 0000-0001-8285-4787
Tyler B. Martin: 0000-0001-7253-6507
Eric M. Davis: 0000-0002-5633-5489

Notes

The authors declare no competing financial interest.

■ ACKNOWLEDGMENTS

This work was supported by Clemson University Department of Chemical and Biomolecular Engineering start-up funds. Allison Domhoff acknowledges financial support from the National Science Foundation Graduate Research Fellowship Program under Grant 1246875. The authors also gratefully acknowledge funding from the National Science Foundation via Award DMR-1848347 and to the Clemson University Advanced Materials Research Lab for use of their facilities. We also acknowledge the support of the National Institute of Standards and Technology, U.S. Department of Commerce, in providing the neutron research facilities used in this work.

■ REFERENCES

(1) Mauritz, K. A.; Moore, R. B. State of Understanding of Nafion. *Chem. Rev.* **2004**, *104*, 4535−4586.

(2) Borup, R.; Meyers, J.; Pivovar, B.; Kim, Y. S.; Mukundan, R.; Garland, N.; Myers, D.; Wilson, M.; Garzon, F.; Wood, D.; Zelenay, P.; More, K.; Stroh, K.; Zawodzinski, T.; Boncella, J.; McGrath, J. E.; Inaba, M.; Miyatake, K.; Hori, M.; Ota, K.; Ogumi, Z.; Miyata, S.; Nishikata, A.; Siroma, Z.; Uchimoto, Y.; Yasuda, K.; Kimijima, K.; Iwashita, N. Scientific Aspects of Polymer Electrolyte Fuel Cell Durability and Degradation. *Chem. Rev.* **2007**, *107*, 3904−3951.

(3) Davis, E. M.; Kim, J.; Oleshko, V. P.; Page, K. A.; Soles, C. L. Uncovering the Structure of Nafion-SiO_2 Hybrid Ionomer Membranes for Prospective Large-Scale Energy Storage Devices. *Adv. Funct. Mater.* **2015**, *25*, 4064−4075.

(4) Trogadas, P.; Pinot, E.; Fuller, T. F. Composite, Solvent-Casted Nafion Membranes for Vanadium Redox Flow Batteries. *Electrochem. Solid-State Lett.* **2012**, *15*, A5−A8.

(5) Skyllas-Kazacos, M.; Kasherman, D.; Hong, D. R.; Kazacos, M. Characteristics and Performance of 1 KW UNSW Vanadium Redox Battery. *J. Power Sources* **1991**, *35*, 399−404.

(6) Tang, Z.; Keith, R.; Aaron, D. S.; Lawton, J. S.; Papandrew, A. P.; Zawodzinski, T. A., Jr. Proton Exchange Membrane Performance Characterization in VRFB. *220th ECS Meeting* **2011**, *41*, 25−34.

(7) Allen, F. I.; Comolli, L. R.; Kusoglu, A.; Modestino, M. A.; Minor, A. M.; Weber, A. Z. Morphology of Hydrated As-Cast Nafion Revealed through Cryo Electron Tomography. *ACS Macro Lett.* **2015**, *4*, 1−5.

(8) Xi, J.; Wu, Z.; Qiu, X.; Chen, L. Nafion/SiO_2 Hybrid Membrane for Vanadium Redox Flow Battery. *J. Power Sources* **2007**, *166*, 531−536.

(9) Dunn, B.; Kamath, H.; Tarascon, J.-M. Electrical Energy Storage for the Grid: A Battery of Choices. *Science* **2011**, *334*, 928−935.

(10) Mai, Z.; Zhang, H.; Li, X.; Xiao, S.; Zhang, H. Nafion/Polyvinylidene Fluoride Blend Membranes with Improved Ion Selectivity for Vanadium Redox Flow Battery Application. *J. Power Sources* **2011**, *196*, 5737−5741.

(11) Luo, Q.; Zhang, H.; Chen, J.; Qian, P.; Zhai, Y. Modification of Nafion Membrane Using Interfacial Polymerization for Vanadium Redox Flow Battery Applications. *J. Membr. Sci.* **2008**, *311*, 98−103.

(12) Lu, S.; Wu, C.; Liang, D.; Tan, Q.; Xiang, Y. Layer-by-Layer Self-Assembly of Nafion−[CS−PWA] Composite Membranes with Suppressed Vanadium Ion Crossover for Vanadium Redox Flow Battery Applications. *RSC Adv.* **2014**, *4*, 24831−24837.

(13) Teng, X.; Zhao, Y.; Xi, J.; Wu, Z.; Qiu, X.; Chen, L. Nafion/Organic Silica Modified TiO_2 Composite Membrane for Vanadium Redox Flow Battery via in Situ Sol−Gel Reactions. *J. Membr. Sci.* **2009**, *341*, 149−154.

(14) Mauritz, K. A.; Warren, R. M. Microstructural Evolution of a Silicon Oxide Phase in a Perfluorosulfonic Acid Ionomer by an in Situ Sol-Gel Reaction. 1. Infrared Spectroscopic Studies. *Macromolecules* **1989**, *22*, 1730−1734.

(15) Antonucci, P. L.; Aricò, A. S.; Cretì, P.; Ramunni, E.; Antonucci, V. Investigation of a Direct Methanol Fuel Cell Based on a Composite Nafion®-Silica Electrolyte for High Temperature Operation. *Solid State Ionics* **1999**, *125*, 431−437.

(16) Mauritz, K. A.; Stefanithis, I. D. Microstructural Evolution of a Silicon Oxide Phase in a Perfluorosulfonic Acid Ionomer by an in Situ Sol-Gel Reaction. 2. Dielectric Relaxation Studies. *Macromolecules* **1990**, *23*, 1380−1388.

(17) Ladewig, B. P.; Knott, R. B.; Hill, A. J.; Riches, J. D.; White, J. W.; Martin, D. J.; Diniz da Costa, J. C.; Lu, G. Q. Physical and Electrochemical Characterization of Nanocomposite Membranes of Nafion and Functionalized Silicon Oxide. *Chem. Mater.* **2007**, *19*, 2372−2381.

(18) Stonehart, P.; Watanabe, M. Polymer Solid-Electrolyte Composition and Electrochemical Cell Using the Composition. 5523181, June 1996.

(19) Dimitrova, P.; Friedrich, K. A.; Stimming, U.; Vogt, B. Modified Nafion®-Based Membranes for Use in Direct Methanol Fuel Cells. *Solid State Ionics* **2002**, *150*, 115−122.

(20) Jansto, A.; Davis, E. M. Role of Surface Chemistry on Nanoparticle Dispersion and Vanadium Ion Crossover in Nafion Nanocomposite Membranes. *ACS Appl. Mater. Interfaces* **2018**, *10*, 36385−36397.

(21) Lin, C.-H.; Yang, M.-C.; Wei, H.-J. Amino-Silica Modified Nafion Membrane for Vanadium Redox Flow Battery. *J. Power Sources* **2015**, *282*, 562−571.

(22) Teng, X.; Zhao, Y.; Xi, J.; Wu, Z.; Qiu, X.; Chen, L. Nafion/Organically Modified Silicate Hybrids Membrane for Vanadium Redox Flow Battery. *J. Power Sources* **2009**, *189*, 1240−1246.

(23) Dresch, M. A.; Matos, B. R.; Fonseca, F. C.; Santiago, E. I.; Carmo, M.; Lanfredi, A. J. C.; Balog, S. Small-Angle X-Ray and Neutron Scattering Study of Nafion-SiO_2 Hybrid Membranes Prepared in Different Solvent Media. *J. Power Sources* **2015**, *274*, 560−567.

(24) Balazs, A. C.; Emrick, T.; Russell, T. P. Nanoparticle Polymer Composites: Where Two Small Worlds Meet. *Science* **2006**, *314*, 1107−1110.

(25) Kumar, S. K.; Jouault, N.; Benicewicz, B.; Neely, T. Nanocomposites with Polymer Grafted Nanoparticles. *Macromolecules* **2013**, *46*, 3199−3214.

(26) Chung, H.-J.; Kim, J.; Ohno, K.; Composto, R. J. Controlling the Location of Nanoparticles in Polymer Blends by Tuning the Length and End Group of Polymer Brushes. *ACS Macro Lett.* **2012**, *1*, 252−256.

(27) Verwey, E. J. W.; Overbeek, J. T. G. *Theory of the Stability of Lyophobic Colloids*; Courier Corporation: 1999.

(28) Napper, D. H. Steric Stabilization. *J. Colloid Interface Sci.* **1977**, *58*, 390−407.

DOI: 10.1021/acsaem.9b01443
ACS Appl. Energy Mater. 2019, 2, 8535−8549

(29) Fritz, G.; Schädler, V.; Willenbacher, N.; Wagner, N. J. Electrosteric Stabilization of Colloidal Dispersions. *Langmuir* **2002**, *18*, 6381−6390.
(30) Rong, M. Z.; Zhang, M. Q.; Ruan, W. H. Surface Modification of Nanoscale Fillers for Improving Properties of Polymer Nanocomposites: A Review. *Mater. Sci. Technol.* **2006**, *22*, 787−796.
(31) Razmjou, A.; Mansouri, J.; Chen, V. The Effects of Mechanical and Chemical Modification of TiO_2 Nanoparticles on the Surface Chemistry, Structure and Fouling Performance of PES Ultrafiltration Membranes. *J. Membr. Sci.* **2011**, *378*, 73−84.
(32) Martin, T. B.; Mongcopa, K. I. S.; Ashkar, R.; Butler, P.; Krishnamoorti, R.; Jayaraman, A. Wetting−Dewetting and Dispersion−Aggregation Transitions Are Distinct for Polymer Grafted Nanoparticles in Chemically Dissimilar Polymer Matrix. *J. Am. Chem. Soc.* **2015**, *137*, 10624−10631.
(33) Cheng, S.; Grest, G. S. Dispersing Nanoparticles in a Polymer Film via Solvent Evaporation. *ACS Macro Lett.* **2016**, *5*, 694−698.
(34) Pourafshari Chenar, M.; Rajabi, H.; Pakizeh, M.; Sadeghi, M.; Bolverdi, A. Effect of Solvent Type on the Morphology and Gas Permeation Properties of Polysulfone−Silica Nanocomposite Membranes. *J. Polym. Res.* **2013**, *20*, 216.
(35) Taurozzi, J. S.; Arul, H.; Bosak, V. Z.; Burban, A. F.; Voice, T. C.; Bruening, M. L.; Tarabara, V. V. Effect of Filler Incorporation Route on the Properties of Polysulfone−Silver Nanocomposite Membranes of Different Porosities. *J. Membr. Sci.* **2008**, *325*, 58−68.
(36) Kumar, S. K.; Benicewicz, B. C.; Vaia, R. A.; Winey, K. I. *50th Anniversary Perspective*: Are Polymer Nanocomposites Practical for Applications? *Macromolecules* **2017**, *50*, 714−731.
(37) Jouault, N.; Zhao, D.; Kumar, S. K. Role of Casting Solvent on Nanoparticle Dispersion in Polymer Nanocomposites. *Macromolecules* **2014**, *47*, 5246−5255.
(38) Liu, Y.-L.; Hsu, C.-Y.; Su, Y.-H.; Lai, J.-Y. Chitosan−Silica Complex Membranes from Sulfonic Acid Functionalized Silica Nanoparticles for Pervaporation Dehydration of Ethanol−Water Solutions. *Biomacromolecules* **2005**, *6*, 368−373.
(39) Tricoli, V. Proton and Methanol Transport in Poly (Perfluorosulfonate) Membranes Containing Cs+ and H+ Cations. *J. Electrochem. Soc.* **1998**, *145*, 3798−3801.
(40) Schneider, C. A.; Rasband, W. S.; Eliceiri, K. W. NIH Image to ImageJ: 25 Years of Image Analysis. *Nat. Methods* **2012**, *9*, 671−675.
(41) Equipment and instruments or materials are identified in the paper in order to adequately specify the experimental details. Such identification does not imply recommendation by the National Institute of Standards and Technology (NIST), nor does it imply the materials are necessarily the best available for the purpose.
(42) Kline, S. R. Reduction and Analysis of SANS and USANS Data Using IGOR Pro. *J. Appl. Crystallogr.* **2006**, *39*, 895−900.
(43) Gill, C.; Price, B.; Jones, C. Sulfonic Acid-Functionalized Silica-Coated Magnetic Nanoparticle Catalysts. *J. Catal.* **2007**, *251*, 145−152.
(44) Peña, L.; Xu, F.; Hohn, K. L.; Li, J.; Wang, D. Propyl-Sulfonic Acid Functionalized Nanoparticles as Catalyst for Pretreatment of Corn Stover. *J. Biomater. Nanobiotechnol.* **2014**, *05*, 8−16.
(45) Howarter, J. A.; Youngblood, J. P. Optimization of Silica Silanization by 3-Aminopropyltriethoxysilane. *Langmuir* **2006**, *22*, 11142−11147.
(46) Kang, T.; Lee, J. H.; Oh, S.-G. Dispersion of Surface-Modified Silica Nanoparticles in Polyamide-Imide (PAI) Films for Enhanced Mechanical and Thermal Properties. *J. Ind. Eng. Chem.* **2017**, *46*, 289−297.
(47) Safari, J.; Zarnegar, Z. An Environmentally Friendly Approach to the Green Synthesis of Azo Dyes in the Presence of Magnetic Solid Acid Catalysts. *RSC Adv.* **2015**, *5*, 17738−17745.
(48) Pham, K. N.; Fullston, D.; Sagoe-Crentsil, K. Surface Charge Modification of Nano-Sized Silica Colloid. *Aust. J. Chem.* **2007**, *60*, 662.
(49) Kim, K.-M.; Kim, H. M.; Lee, W.-J.; Lee, C.-W.; Kim, T.; Lee, J.-K.; Jeong, J.; Paek, S.-M.; Oh, J.-M. Surface Treatment of Silica Nanoparticles for Stable and Charge-Controlled Colloidal Silica. *Int. J. Nanomed.* **2014**, *9*, 29−40.
(50) Clogston, J. D.; Patri, A. K. Zeta Potential Measurement. In *Characterization of Nanoparticles Intended for Drug Delivery; Methods in Molecular Biology*; Humana Press: 2011; pp 63−70.
(51) Mafe, S.; Ramirez, P.; Tanioka, A.; Pellicer, J. Model for Counterion-Membrane-Fixed Ion Pairing and Donnan Equilibrium in Charged Membranes. *J. Phys. Chem. B* **1997**, *101*, 1851−1856.
(52) Donnan, F. G. Theory of Membrane Equilibria and Membrane Potentials in the Presence of Non-Dialysing Electrolytes. A Contribution to Physical-Chemical Physiology. *J. Membr. Sci.* **1995**, *100*, 45−55.
(53) Balwani, A.; Faraone, A.; Davis, E. M. Impact of Nanoparticles on the Segmental and Swelling Dynamics of Ionomer Nanocomposite Membranes. *Macromolecules* **2019**, *52*, 2120−2130.
(54) Hsu, W. Y.; Gierke, T. D. Ion Transport and Clustering in Nafion Perfluorinated Membranes. *J. Membr. Sci.* **1983**, *13*, 307−326.
(55) Vijayakumar, M.; Luo, Q.; Lloyd, R.; Nie, Z.; Wei, X.; Li, B.; Sprenkle, V.; Londono, J.-D.; Unlu, M.; Wang, W. Tuning the Perfluorosulfonic Acid Membrane Morphology for Vanadium Redox-Flow Batteries. *ACS Appl. Mater. Interfaces* **2016**, *8*, 34327−34334.
(56) Wang, X.; Tilley, R. D.; Watkins, J. J. Simple Ligand Exchange Reactions Enabling Excellent Dispersibility and Stability of Magnetic Nanoparticles in Polar Organic, Aromatic, and Protic Solvents. *Langmuir* **2014**, *30*, 1514−1521.
(57) Bansal, A.; Yang, H.; Li, C.; Benicewicz, B. C.; Kumar, S. K.; Schadler, L. S. Controlling the Thermomechanical Properties of Polymer Nanocomposites by Tailoring the Polymer−Particle Interface. *J. Polym. Sci., Part B: Polym. Phys.* **2006**, *44*, 2944−2950.
(58) Neutron Activation and Scattering Calculator; https://www.ncnr.nist.gov/resources/activation/ (accessed Sept 26, 2018).
(59) Loppinet, B.; Gebel, G.; Williams, C. E. Small-Angle Scattering Study of Perfluorosulfonated Ionomer Solutions. *J. Phys. Chem. B* **1997**, *101*, 1884−1892.
(60) Rubatat, L.; Rollet, A. L.; Gebel, G.; Diat, O. Evidence of Elongated Polymeric Aggregates in Nafion. *Macromolecules* **2002**, *35*, 4050−4055.
(61) Gebel, G.; Diat, O. Neutron and X-Ray Scattering: Suitable Tools for Studying Ionomer Membranes. *Fuel Cells* **2005**, *5*, 261−276.
(62) Gebel, G.; Lambard, J. Small-Angle Scattering Study of Water-Swollen Perfluorinated Ionomer Membranes. *Macromolecules* **1997**, *30*, 7914−7920.
(63) Kim, K. D.; Sperling, L. H.; Klein, A.; Wignall, G. D. Characterization of Film Formation from Direct Miniemulsified Polystyrene Latex Particles via SANS. *Macromolecules* **1993**, *26*, 4624−4631.
(64) Balasoiu, M.; Anitas, E. M.; Bica, I.; Osipov, V. A.; Orelovich, O. L.; Savu, D.; Savu, S.; Erhan, R.; Kuklin, A. I. SANS of Interacting Magnetic Micro-Sized Fe Particles in a Stomaflex Creme Polymer. *Matrix. Optoelectron. Adv. Mater.* **2008**, *2*, 730−734.
(65) Spohr, E.; Commer, P.; Kornyshev, A. A. Enhancing Proton Mobility in Polymer Electrolyte Membranes: Lessons from Molecular Dynamics Simulations. *J. Phys. Chem. B* **2002**, *106*, 10560−10569.
(66) Wang, Y.; Agapov, A. L.; Fan, F.; Hong, K.; Yu, X.; Mays, J.; Sokolov, A. P. Decoupling of Ionic Transport from Segmental Relaxation in Polymer Electrolytes. *Phys. Rev. Lett.* **2012**, *108*, 2717−2727.
(67) Hickner, M. A. Water-Mediated Transport in Ion-Containing Polymers. *J. Polym. Sci., Part B: Polym. Phys.* **2012**, *50*, 9−20.

DOI: 10.1021/acsaem.9b01443
ACS Appl. Energy Mater. 2019, 2, 8535−8549